frontiers | Frontiers in Astronomy and Space Sciences

TYPE Original Research
PUBLISHED 24 June 2025
DOI 10.3389/fspas.2025.1530408

OPEN ACCESS

EDITED BY
Andrea Longobardo,
National Institute of Astrophysics (INAF), Italy

REVIEWED BY
Gerhard Paar,
Joanneum Research, Austria
Robert Barnes,
Imperial College London, United Kingdom

*CORRESPONDENCE
Gabriela Ligeza,
gabriela.ligeza@unibas.ch

RECEIVED 18 November 2024
ACCEPTED 26 May 2025
PUBLISHED 24 June 2025

CITATION
Ligeza G, Bontognali TRR, Fayon L, Bouquety A, Hofmann B, Josset J-L and Kuhn NJ (2025) Close - up imaging of Oxia Planum analogue samples under different illumination conditions: preparing for the ExoMars rover mission.
Front. Astron. Space Sci. 12:1530408.
doi: 10.3389/fspas.2025.1530408

Close - up imaging of Oxia Planum analogue samples under different illumination conditions: preparing for the ExoMars rover mission

Gabriela Ligeza[1]*, Tomaso R. R. Bontognali[1,2], Lucile Fayon[2], Axel Bouquety[2], Beda Hofmann[3,4], Jean-Luc Josset[2] and Nikolaus J. Kuhn[1]

[1]Department of Environmental Sciences, Physical Geography and Environmental Change Group, University of Basel, Basel, Switzerland, [2]Space Exploration Institute, Neuchâtel, Switzerland, [3]Natural History Museum, Bern, Switzerland, [4]Institute of Geological Sciences, University of Bern, Bern, Switzerland

ExoMars is an astrobiology program led by the European Space Agency, which foresees the launch of a rover that will look for signs of past life on Mars. CLUPI, a close-up imager part of the rover's payload, is designed for capturing high-resolution images of geological samples. Ensuring that each CLUPI image contains a maximum of relevant scientific information is crucial for optimizing the scientific return of the instrument and for the daily tactical planning of the rover's activities. This study focuses on identifying the preferred lighting conditions for close-up image acquisition in the area that will be explored by the rover: Oxia Planum. To identify lithologies potentially occurring in this region, we conducted a comprehensive review of past publications on Oxia Planum's mineralogy and geology and analysed image repositories from previous rover missions to guide our selection of samples relevant to the ExoMars mission. These samples were chosen either because we anticipate their presence at the landing site or because they represent highly interesting targets in a mission primarily aimed at finding potential evidence of past microbial life. The samples were categorized into five groups: 1) clastic sedimentary rocks, 2) rocks with Fe-Mg phyllosilicates, 3) igneous rocks, 4) evaporites, carbonates and morphological biosignatures, and 5) rocks with various sedimentary structures. For each group, we identified diagnostic textures visible in CLUPI images. The rocks were photographed using a CLUPI analogue camera under Mars - simulated lighting conditions, varying the proportion of direct and indirect light to mimic morning, evening, and mid-day conditions on Mars, as well as during dust storm conditions. We demonstrated that strategically capturing images at different times of the day under specific illuminations enhances the likelihood of detecting diverse rock textures and relevant structures. Moreover, the images produced in our simulations constitute a reference dataset of Oxia-analogue samples. Thereby, they support the exploration strategy for CLUPI and will help the science team in the decision-making process and data interpretation during the prime mission on Mars.

KEYWORDS

ExoMars, CLUPI, operational strategy, analogue rocks, Oxia Planum

1 Introduction

The ExoMars Rosalind Franklin Rover mission is part of an astrobiology program led by the European Space Agency (ESA), with the main goal of searching for evidence of past life on Mars (Vago et al., 2017). While the mission's core focus is astrobiology, specifically studying whether there was active life at Oxia Planum, it encompasses several secondary objectives. These include investigating the possibility of hydrothermal springs at Oxia during the Noachian period, the formation mechanisms of phyllosilicates and other water-related minerals, as well as third-priority questions such as hydrothermal activity and volcanism, general surface conditions, aeolian processes, and overall surface conditions to unravel the planet's evolution and ancient climate (Sefton-Nash and Vago, 2024).

In contrast to previous Mars rover missions, the ExoMars rover will be equipped with a drill capable of obtaining samples from depths of up to 2 m, increasing the likelihood of detecting intact biomarkers that were not degraded by the intense cosmic radiation hitting the surface (Vago et al., 2015). To conduct in-depth geological observations and identify potential biosignatures, the ExoMars Rosalind Franklin rover is equipped with a diverse set of instruments, including cameras: Panoramic Camera - PanCam (Coates et al., 2017); and Close-Up Imager–CLUPI (Josset et al., 2017) and three Near-Infrared (NIR) instruments: ENFYS - a new infrared spectrometer, which replaces ISEM-Infrared Spectrometer for ExoMars (Korablev et al., 2017), Mars Multispectral Imager for Subsurface Studies - Ma_MISS (De Sanctis et al., 2017), and a visible near-infrared hyperspectral microscope - MicrOmega; (Bibring et al., 2017). Additionally, the mission includes the Mars Organic Molecule Analyser–MOMA (Goesmann et al., 2017), the Raman Spectrometer–RLS (Rull et al., 2017), and the Water Ice and Subsurface Deposit Observation on Mars–WISDOM (Ciarletti et al., 2017).

The Close Up-imager CLUPI will play a crucial role in the exploration cascade by providing close-up images of geological outcrops and Martian regolith. Information from these images will be used by the science team to make decisions regarding further in-depth mineralogical and geochemical analysis. CLUPI is located on the movable drill box (Figure 1A), allowing for the acquisition of images from various angles and additional views are possible thanks to two mirrors (Josset et al., 2017). Depending on the operation configuration and the mirror used, CLUPI images correspond to three different fields of view (FOV): FOV 1–2,652 × 1768 pixels; FOV 2 - 2,652 × 1,128 pixels, and FOV 3 - 2,652 × 640 pixels (Figure 1B). This enables the acquisition of RGB colour images in operation modes referred to as: geological environment surveys, close-up outcrop observations, observations of the drilling area/drill hole, and drill core samples imaging (Josset et al., 2017).

CLUPI will be able to perform z-stacking (or focus stacking) of images, when necessary, to increase the scientific return. Z-stacking is a processing technique that combines multiple images taken at different focus distances, resulting in an extended depth of field and enhanced image clarity (Josset et al., 2017). The instrument can also perform autoexposure and autofocus, valuable for providing detailed morphological information essential to geological interpretations. CLUPI can focus from 10 cm to infinity (Josset et al., 2017). At a distance of 10 cm from the target object, the resolution of the images will be approximately 7 μm/pixel, allowing the camera to capture fine details such as grains, thin laminations, and complex rock textures. Furthermore, despite CLUPI having a single optical group, it will be possible to use it to obtain 3D images by capturing photographs of the same target after moving the rover (Bouquety et al., 2024). This feature can be used to produce scaled 3D models for measurement of geomorphological and sedimentary structures at various scale.

Taking into account that the Rosalind Franklin rover is equipped with a total of 8 cameras to assist navigation and that the MaMiss, MicrOmega, and RLS instruments are also equipped with imaging systems, the majority of images expected to be acquired during the mission to characterize the geology of Oxia Planum will be captured using PanCam and CLUPI (Vago et al., 2017). PanCam will be the prime tool for characterising the morphology and geology of rock outcrops and large-scale features on the Martian surface, playing a crucial role in geological target selection and initial site characterisation (Coates et al., 2017). CLUPI, on the other hand, will provide essential close-up visual (Josset et al., 2017), enabling the detailed assessment of hypotheses and planning of proximity science, such as evaluating potential drill sites.

Due to data transmission limitations, the science team will receive only a few CLUPI images per day. As the sole source of such high-resolution, close-up imagery, CLUPI data will be critical for refining decisions and planning rover activities in subsequent cycles. Therefore, it is essential that each CLUPI image contains a maximum of relevant information to optimise the scientific return.

Building on previous CLUPI science validation and mission preparatory activities (Hickman-Lewis et al., 2020; Bontognali et al., 2021; Foucher et al., 2022), this study further investigates the impact of various illumination conditions on the detection of Oxia planum specific rock textures and sedimentary structures in close-up images produced by a CLUPI analogue camera (i.e., a commercial camera and lens produced by Canon, which allowed us to simulate CLUPI's field of view but has differences in both detector technology and optical group (see section 2.3). The experimental simulations were conducted simulations in the Marslabor of the University of Basel and at the Space Exploration Institute laboratory in Neuchâtel (SEI Lab, Microcity, Neuchâtel, Switzerland). The CLUPI analogue camera was used to evaluate how varying illumination scenarios affect the visibility and differentiation of geological features. Close-up images of geological samples were captured under

10.3389/fspas.2025.1530408

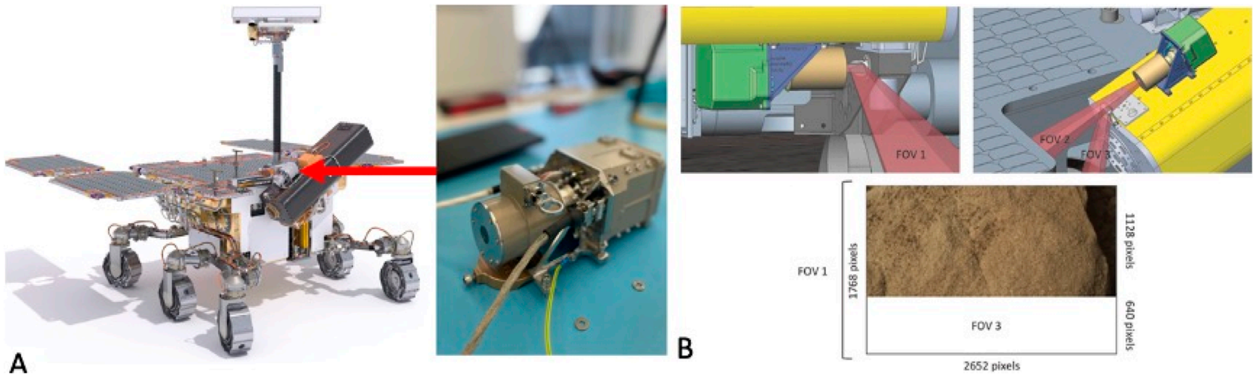

FIGURE 1
(A) The CLUPI instrument on the movable drill box, **(B)** Three different fields of view of CLUPI, after Josset et al., 2017 with the image of sandstone (FOV 2) acquired with the CLUPI EM + model.

diverse lighting conditions, including morning and evening light characterized by a low solar angle, midday light with a high solar angle, and diffused lighting conditions where sunlight is scattered in the Martian atmosphere, creating a soft, evenly spread illumination rather than direct, harsh lighting. The concept developed in this study will be valuable for future CLUPI science validation activities, as well as for the science team in image acquisition and decision-making during the primary mission on Mars.

2 Methods

2.1 Oxia Planum and rock sample selection

The ExoMars rover is expected to land within the Oxia Planum region, which is known to have a geologically diverse terrain, including a stratified bedrock with hydrous phyllosilicates of Noachian age, which likely formed in the presence of water (Mandon et al., 2019), several igneous units, and fluvial and deltaic deposits (Quantin-Nataf et al., 2021; Vago et al., 2017; Davis et al., 2023). To identify the lithologies potentially occurring in this region, we conducted a comprehensive review of past publications on Oxia Planum's mineralogy and geology (e.g., Quantin-Nataf et al., 2021; Mandon et al., 2021; Hauber et al., 2021; Brossier et al., 2022) and we considered the publicly available image data repository of Curiosity and Perseverance rovers at https://mars.nasa.gov/to gain an overview of the textures that might be encountered on the Martian surface. We also examined The Planetary Terrestrial Analogues Library (PTAL) as a potential analogue for Martian rocks (Veneranda et al., 2021; Krzesińska et al., 2021).

The samples for this study were provided by several research collections: the University of Basel research collection, the Natural History Museum Bern (NMBE), the Planetary Terrestrial Analogues Library at the University of Oslo (PTAL) and by the Space Exploration Institute of Neuchatel collection. Additionally, some samples collected during fieldwork in the Eifel Volcanic Field in Germany, organized within the scope of this study, and during previous fieldwork in Qatar to sample gypsum and microbial mats, as well as in the Pilbara region of Australia, where the stromatolites were collected.

2.2 Simulation of variable lighting conditions for CLUPI's daily operations on mars

Selected samples were photographed at the Marslabor of the University of Basel, an indoor facility with a testbed comprised of basalt that simulates a Martian landscape and an illumination system (Bontognali et al., 2021). We simulated operational scenarios in which the rover could capture images during various phases of the Martian daily cycle, including mid-day illumination (Figure 2A), evening, and morning conditions (Figure 2B), and diffused lighting (Figure 2C). For midday conditions (Figure 2A), we assumed a high solar angle of approximately 70°, with the Sun near zenith. Under such conditions, light arrives from a steeper angle, resulting in shorter shadows and more direct illumination, which can reduce contrast and flatten the appearance of surface textures. In evening/morning conditions (Figure 2B), we applied a low solar angle of approximately 25°, representing the Sun closer to the horizon. This lower angle causes light to arrive at a shallower incidence, producing elongated shadows and emphasising surface textures and topographic relief. For diffused lighting (Figure 2C), we considered scenarios typical of dust storms or periods of high atmospheric dust loading. In these cases, sunlight is mostly scattered by dust particles suspended in the atmosphere, creating a soft, evenly spread illumination that reduces shadow contrast while enhancing uniform brightness across the scene.

To achieve the simulated lighting conditions for both direct (midday) and indirect (evening/morning) scenarios, we adjusted the positioning of lamps (Figure 2D) and modulated their power outputs to provide measured values of 5,000 lux for direct light and 1,000 lux for diffused light on the sample surface. A 5:1 direct-to-diffused light ratio represents an end-member in the spectrum of possible lighting conditions on Mars, where direct light is particularly dominant. This scenario allows for the production of images where the differences between mid-day light, sunset light,

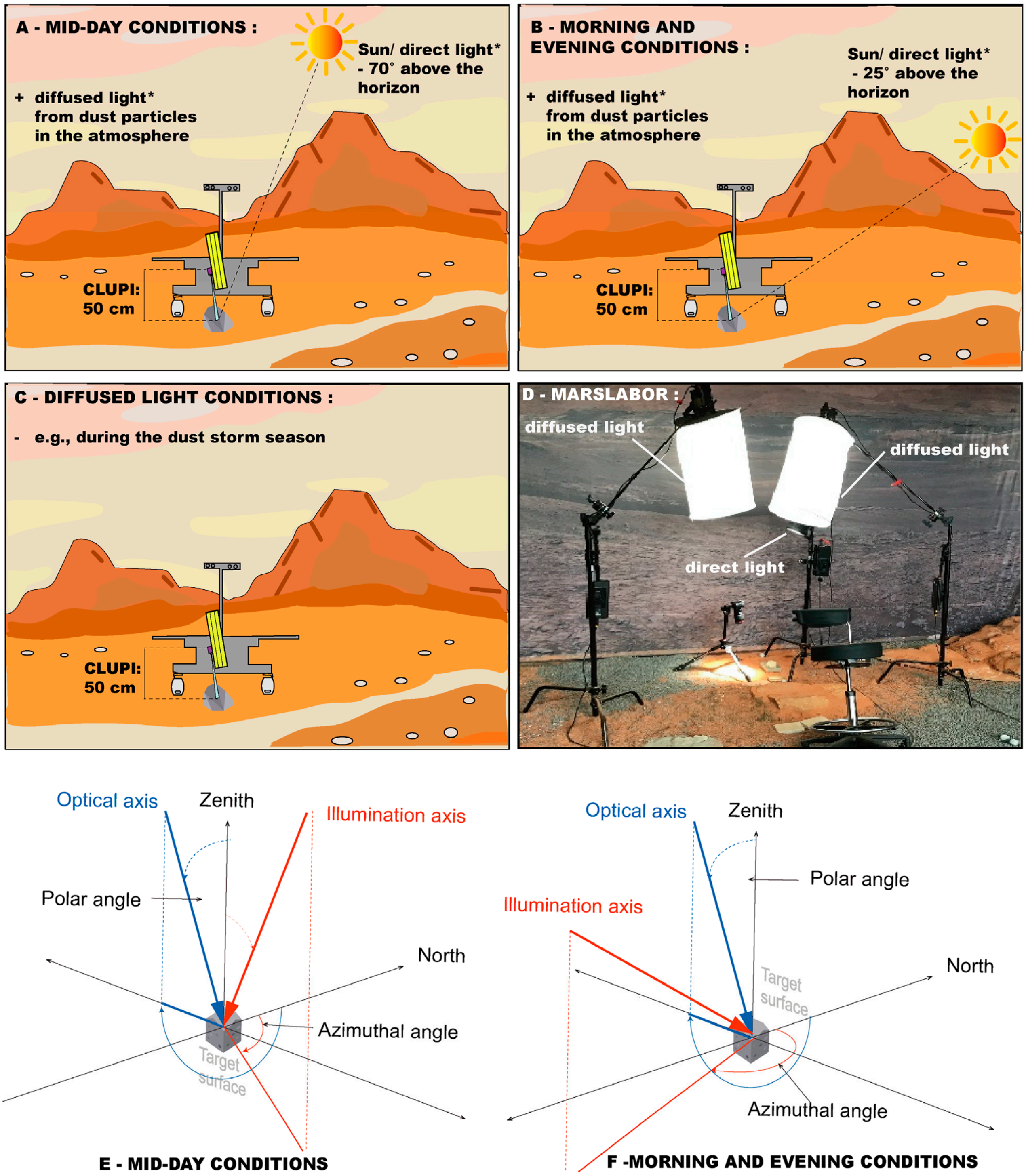

FIGURE 2
Experimental set-up in the Marslabor - **(A)** Mid-day condition with a solar angle of 70°. **(B)** Morning/evening condition with a solar angle of 25°. **(C)** Dust storm conditions with the diffused light only. **(D)** Marslabor set-up, illustrating the ratio of direct to indirect (diffused) light (5,000:1000 LUX) for mid-day, morning, and evening conditions and only 1000 LUX for the dust storm conditions with CLUPI's working distance (50 cm). **(E,F)** spherical reference system (modified after Bontognali et al., 2021) for mid-day **(E)** and morning and evening conditions **(F)**. The system is used to describe the optical axis (i.e., the "line between the camera and the centre of the target surface") and the illumination axis (i.e., the "line between the direct light source and the centre of the target surface"). The origin of the reference system is the centre of the target surface, and the reference plane is the horizontal plane (parallel to the floor of the Marslabor). The polar angle is measured from the zenith, and the azimuthal angle is measured from the North in clockwise direction. The orientation of the target surface is described using the dip and strike notation. All rocks in this study were horizontal to the reference plane; therefore, their dip and strike are always 0°).

and only diffused light are more pronounced. However, although such a ratio is possible under exceptionally clear skies and minimal dust, it rarely occurs because the pervasive fine dust particles in Mars atmosphere scatter sunlight effectively, typically resulting in a much higher proportion of diffused light (Appelbaum and Flood, 1990; Appelbaum et al., 1993). Diffuse light primarily results from sunlight interacting with suspended dust particles through Mie and Rayleigh scattering (e.g., Egan and Foreman, 1971) which softens direct sunlight and spreads it across the sky, contributing to the diffuse, reddish ambient glow characteristic of daytime on Mars. This effect becomes more pronounced during dust storms but remains minimal in non-dusty conditions when the Sun is near zenith (Pollack et al., 1979). In our study, we simulated white light conditions to focus on the effects of illumination on shadow formation and surface contrast rather than colour representation. White light, containing a balanced spectrum of all visible wavelengths, was chosen to minimise the influence of colour variations and instead emphasise how different lighting angles and intensities affect the visibility of geological features. This approach allowed us to assess the role of direct and diffuse light in revealing surface textures, shadows, and topographic relief, which are critical for the scientific analysis of rock targets at Oxia Planum. Nevertheless, we acknowledge that our lamp setup is far from providing an accurate simulation of the lighting conditions on Mars at different times of the day. For this purpose, it would be necessary to consider not only the illumination axis and the ratio of direct to diffused light but also spectral variations (Thomas et al., 1999).

All images were acquired to simulate CLUPI's Field of View 2 (FOV 2) at the "drill area high position" (Josset et al., 2017), with a working distance of 50 cm (Figure 2) and resolution of 39 µm/pixel. This field of view corresponds to one of the most common CLUPI's close-up outcrops observation configuration, anticipated for the primary mission, before decisions regarding drilling and further analytical investigations are made (Josset et al., 2017). We acquired all images with the same FOV 2 and working distance to produce a homogeneous image dataset for the study. To mimic the position of the CLUPI on the rover's drill box, we fixed camera on a tripod to replicate the drill's high position, maintaining an incidence angle of 11° (Josset et al., 2017) (Figure 2D).

To orient the samples, we used the spherical reference system as described by Bontognali et al. (2021). Here, the term "target surface" (Figures 2E,F) refers to the plane that defines the spatial orientation of the region of interest, which in the case of this study, is the rock sample placed horizontally on the ground within the regolith. The optical axis (i.e., the "line between the camera and the centre of the target surface" or the "direction from which the image is taken") is represented using a spherical coordinate system (Figures 2E,F), with the origin being the centre of the target surface and the reference plane as the horizontal plane (parallel to the floor of the Marslabor), orthogonal to the zenith. The polar angle is measured from the zenith, while the azimuthal angle is measured from the North in a clockwise direction. The illumination axis (i.e., the line between the direct light source and the centre of the target surface) is also represented using the same spherical coordinate system (Figures 2E,F) used to define the optical axis. We have also artificially set the North to correspond to the back wall of the Marslabor and placed all the photographed samples parallel to it. In this study, all samples were placed horizontally; therefore, they all have a dip and strike of 0°. For the mid-day conditions (Figure 2E), the illumination axis has a polar angle of 20° and an azimuthal angle of 90°, while the optical axis has a polar angle of 78.5° and an azimuthal angle of 270°. For the morning/evening conditions (Figure 2F), the optical axis maintains a polar angle of 78.5° and an azimuthal angle of 270°, while the illumination axis has a polar angle of 65° and an azimuthal angle of 180°.

2.3 Image acquisition with CLUPI analogue camera and with the EM + engineering model

The system used for this study consists of a Canon EOS M50 equipped with a Canon 110 mm fixed macro lens and an EF-EOS M mount adapter. This setup was chosen for its similarity to CLUPI's specifications in terms of field of view and working distance range, making it one of the most suitable options among commercially available cameras. As the Canon EOS M50 has a detector of 5,196 × 3,464 pixels compared to CLUPI's 2,652 × 1,768 (Josset et al., 2017), all acquired images underwent post-processing in Adobe Photoshop to align their actual spatial resolution with that of CLUPI. To obtain FOV2, we cropped the EOS M50 images in Adobe Photoshop, setting the image size to 2,652 × 1,128 pixels.

It is important to clarify that the Canon EOS M50 camera differs from CLUPI in many aspects, starting with the detector technology (Foveon sensor), which differs from that of the Canon, which uses a Bayer filter. A Foveon sensor captures color information through a layered design, recording all three primary colors at each pixel, while a Bayer sensor (like in the Canon EOS M50) uses a colour filter array, where each pixel captures only one colour and the full image is reconstructed through demosaicing. Furthermore, CLUPI's optical system was specifically designed for this instrument and has different specifications in terms of depth of field, geometric distortions, and chromatic aberrations compared to the Canon lens and other commercially available lenses (Josset et al., 2017). The photographs taken with the Canon camera were captured with an aperture set at f/8, using exposure times ranging from 200 ms to 5 ms. CLUPI does not have a variable diaphragm, and its f-number depends on the working distance. Depending on the working distance, the position of the lenses relative to the detector is adjusted using an autofocus mechanism. This affects the aperture value, which varies approximately between f/9 and f/16. For the 50 cm working distance used in this study, the f-number is approximately 14. The exposure times used for image acquisition ranged between 200 ms and 3,000 ms, with most images acquired at 200 ms.

To ensure that our simulation and conclusions remain relevant for the preparation of the ExoMars mission despite the differences between the two instruments, we conducted tests comparing images from the Canon with those from the CLUPI EM+. Although visible differences exist, mostly due to the fact that the calibration of this instrument is not yet complete, these differences are not significant enough to invalidate or contradict our general conclusions regarding the preferred illumination for visualizing geological samples of interest for the mission. The images used for comparison were acquired with the flight model representative of CLUPI (the EM + model) in the CLUPI Science Operations Laboratory of the Space Exploration Institute based in Neuchatel, (SEI Lab, Microcity, Neuchatel, Switzerland) using similar image acquisition parameters as those for the Canon camera, FOV2 (section 2.2), with a working distance of 50 cm.We conducted tests on two major rock types (Supplementary material, Figure 1) with distinct textures and morphologies: a sandstone with laminations and a basalt with fine phenocrysts. Our results confirm that the identification of phenocrysts and laminations under variable lighting conditions is consistent for both Canon and CLUPI EM+ (Supplementary material, Figure 1).

3 Collection of analogue rocks of Oxia Planum

3.1 Analogue rocks: textures, morphologies, and biosignature preservation potential

In order to identify the preferred lighting conditions for CLUPI to capture relevant textures and rock lithologies, we gathered a total of 30 Oxia Planum analogue rocks for an experimental study (Table 1). We divided them into in five groups: (1) clastic sedimentary rocks (2) rocks with Fe-Mg phyllosilicates, (3) igneous rocks, (4) evaporites, carbonates and morphological biosignatures, and (5) rocks with various morphological features. For each of these groups, we identified the diagnostic textures and morphological features which are supposed to be visible with CLUPI, such as presence of phenocrysts, vesicles, pebbles and grains within clastic sedimentary rocks, desiccation cracks, and alteration veins. Capturing these small-scale features is important as they provide key information for evaluating geological context and assessing the potential for preserving biosignatures in the host rock and, in extraordinary cases, even finding direct morphological biosignatures like stromatolites and other microbially induced sedimentary structures (MISS) (Noffke et al., 2001; Allwood et al., 2013; Allwood et al., 2015; Westall et al., 2015; Davies et al., 2016).

Information about all the samples photographed in this study are summarized in Table 1, where the first two columns show the rock type, followed by textural and morphological features to be captured by CLUPI, information about their origin, geological age and name of formation, accessibility for further analysis, the presence of their equivalent on Mars, their paleoenvironmental significance and their potential to preserve biosignatures.

3.1.1 Clastic sedimentary rocks

One of the primary scientific objectives of the ExoMars mission is to search for signs of life. Consequently, sedimentary rocks that form at low temperatures permitting the presence of liquid water represent a main target for astrobiological sampling (Bosak et al., 2021). Due to the lack of plate tectonics, on Mars these rocks remain relatively unaffected by metamorphism, providing a unique opportunity to discover deposits that may contain and preserve morphological and geochemical biosignatures (Eigenbrode et al., 2018; Bosak et al., 2021; Scheller et al., 2022). Documenting with close-up images the textures and morphological features of sedimentary rocks, such as laminations, stratifications, grain size, shape, and roundness, will therefore be a priority during the ExoMars mission.

The most common types of sedimentary rocks identified by previous Mars rovers associated with aqueous environments include fine-grained laminated mudstones (e.g., Rampe et al., 2017; Eigenbrode et al., 2018; Stack et al., 2019; Simon et al., 2022), sandstones (Grotzinger et al., 2005; Yen et al., 2017; Achilles et al., 2020; Rampe et al., 2020), and conglomerates with rounded grains, suggesting fluvial transport (Williams et al., 2013; Dietrich et al., 2017). One of the most studied clastic sedimentary rocks associated with aeolian and fluvial deposits on Mars is moderately well-rounded sandstone (0.1–1 mm) from the Burns Formation in Meridiani Planum, which is linked to an aeolian depositional system (Grotzinger et al., 2005). Additional examples include sandstone facies with meter-scale bedding at Victoria crater (Hayes et al., 2011) and aeolian deposits in Gale crater, characterized by dunes and ripples within the sandstone (Banham et al., 2018; Banham et al., 2022). Furthermore, diverse sedimentary facies—including fine-grained laminated sandstone, pebbly sandstone, and coarse-grained sandstone—have been identified in the Shaler Formation in Gale crater (Edgar et al., 2018).

Thinly laminated mudstones with low-angle cross-stratifications have also been observed in Gale crater, interpreted as evidence of plunging river plume deposits (Stack et al., 2019). Similar laminated mudstones occur in Jezero crater's Shenandoah Formation, where they are associated with thick-bedded granule-pebble sandstone and conglomerates, suggesting deposition in alluvial fan and deltaic environments (Stack et al., 2024).

Moreover, on Earth, all of these lithologies have been shown to preserve microbial mats when interbedded with mudstones, and even sandstones (e.g., Homann et al., 2018; Homann, 2019). In Oxia Planum, the highest likelihood of finding these rocks would be within fluvial (Fd) and deltaic deposits (Dt) (Quantin-Nataf et al., 2021). These sedimentary rocks could also be found in proximity to topographical features referred to as rounded buttes, which are interpreted to be related to aqueous and erosional processes (McNeil et al., 2021; Fawdon et al., 2022). Moreover, remote sensing observations have detected layered deposits on the walls of the craters (Quantin-Nataf et al., 2021), which could also be directly associated with layered sedimentary rocks.

3.1.2 Rocks with Fe-Mg phyllosilicates

A high-priority task for ExoMars is to analyse rocks rich in Fe-Mg phyllosilicate, which have been detected by orbital spectral analysis at Oxia Planum and likely have formed at low temperature through interactions with water (Mandon et al., 2019). Although the exact nature of Fe-Mg phyllosilicate deposits is not yet known at Oxia Planum, the Fe-Mg phyllosilicates are widespread across the whole landing region, and their layered outcrops are especially exposed on the walls of craters (Quantin-Nataf et al., 2021), suggesting that these types of rocks can be encountered anywhere at Oxia. Mudstones are good rock candidates that may contain Fe-Mg phyllosilicates (e.g., Peretyazhko et al., 2016; Playter et al., 2017). However, Fe-Mg phyllosilicate minerals can also be found as alteration products within igneous rocks, which occur without the sedimentary structures commonly linked to the deposition of detrital clay minerals (Mège et al., 2023). Indeed, on Mars, most of the previously detected phyllosilicates were associated with Noachian outcrops where the igneous minerals

10.3389/fspas.2025.1530408

TABLE 1 Potential analogue rock samples present at Oxia Planum and their geological, paleoenvironmental, and biosignatures preservation potential.

Rock group	Rock type	Textural and morphological features to be captured with CLUPI	Analog sample origin/Information	Geological age and name of formation	Accessibility for further analysis	Previous observations on mars (examples)	Geological history and paleoenvironment	Biosignature preservation potential
1. Clastic sedimentary rocks								
A	Sandstone - coarse-grained (0.5 mm)	Laminations, equigranular texture	Unknown*	Unknown	Yes - via UniBasel	Curiosity and Perseverance rovers (Yen et al., 2017; Achilles et al., 2020; Grotzinger et al., 2005; Bennett et al., 2023; Stack et al., 2023)	fluvial/coastal environement, paleolakes, microbial mats can be interbedded with fluvial sandstones (Homann, 2019)	moderate (Homann, 2019)
A1	Sandstone - coarse-grained (0.25–0.5 mm)	Well-sorted sandstone, sub-rounded	Artifically made on petri dish*	Unknown	Yes - via UniBasel	Curiosity and Perseverance rovers (Yen et al., 2017; Achilles et al., 2020; Grotzinger et al., 2005; Bennett et al., 2023; Stack et al., 2023)	fluvial/coastal environement, paleolakes, microbial mats can be interbedded with fluvial sandstones (Homann, 2019)	moderate (Homann, 2019)
A2	Sandstone - fine-grained (0.1–0.25 mm)	Well-sorted sandstone, sub-rounded	Artifically made on petri dish*	Unknown	Yes - via UniBasel	Curiosity and Perseverance rovers (Yen et al., 2017; Achilles et al., 2020; Grotzinger et al., 2005; Bennett et al., 2023; Stack et al., 2023)	fluvial/coastal environement, paleolakes, microbial mats can be interbedded with fluvial sandstones (Homann, 2019)	moderate (Homann, 2019)
A3	Very fine-grained sandstone (0.06–0.1 mm)	Fine-grained sandstone	Oberkail sandstone and gravel quarry, Germany*	Tertiary period, Miocene epoch, 23–5.3 Ma; Oberkail Formation	Yes - via UniBasel	Curiosity and Perseverance rovers (Yen et al., 2017; Achilles et al., 2020; Grotzinger et al., 2005; Bennett et al., 2023; Stack et al., 2023)	fluvial/coastal environement, paleolakes, microbial mats can be interbedded with fluvial sandstones (Homann, 2019)	moderate (Homann, 2019)
B	Feldspar-rich sandstone	Poorly sorted, angular grains	Unknown*	Unknown	Yes - via UniBasel	Curiosity and Perseverance rovers (Yen et al., 2017)	short transport, high energy environments, e.g., alluvial fans, flood channels (fluvial processes) (Yen et al., 2017)	low

(Continued on the following page)

TABLE 1 (*Continued*) Potential analogue rock samples present at Oxia Planum and their geological, paleoenvironmental, and biosignatures preservation potential.

Rock group	Rock type	Textural and morphological features to be captured with CLUPI	Analog sample origin/Information	Geological age and name of formation	Accessibility for further analysis	Previous observations on mars (examples)	Geological history and paleoenvironment	Biosignature preservation potential
C	Conglomerate	Poorly sorted/sub-rounded clasts	Oberkail sandstone and gravel quarry, Germany*	Tertiary period, Miocene epoch, 23–5.3 Ma; Oberkail Formation	Yes - via UniBasel	Curiosity and Perseverance rovers (Williams et al., 2013; Dietrich et al., 2017; Bosak et al., 2021)	fluvial processes	low
D	Mudstone	Fine laminations	Eifel Volcanic Field, Germany*	Miocene epoch, 23–5.3 Ma; Bellerberg Formation; volcaniclastic sediments	Yes - via UniBasel	Curiosity and Perseverance rovers (Eigenbrode et al., 2018; Rampe et al., 2017; Stack et al., 2019; Mangold et al., 2021)	Might contain phyllosilicates, preserve organic matter, indication of fluvial processes, microbial mats can be interbedded with mudstones (Homann, 2019). Mudstones can also form in marine environments, lacustrine environments, and in some aeolian environments	moderate - high (Bosak et al., 2021)
E	Mudstone	Laminations	Jura, CH*	Late Jurassic to the Early Cretaceous, 160–140 Ma; marine deposits	Yes - via UniBasel	Curiosity and Perseverance rovers (Eigenbrode et al., 2018; Rampe et al., 2017; Stack et al., 2019)	might contain phyllosilicates, preserve organic matter, indication of fluvial processes but lso aeolian or lacustrine (Day-Stirrat et al., 2008)	moderate -high (Bosak et al., 2021)
2.Rocks with FE-MG Phyllosilicates								
A	Altered phonolite	Fe/Mg - phyllosilicates (smectite) in layers (April and Keller, 1992; Robinson and Luttrell, 1985; Schlische, 1993; Krzesińska et al., 2021)	Granby Basaltic Tuff***	Late Triassic to Early Jurassic periods, roughly 200 to 220 Ma; olland Volcanic Series, which is associated with the Hartford Basin	Yes- via PTAL University of Oslo	Spectral signature of these terrestrial rocks match the mineralogy of Oxia Planum clays (OMEGA) (Krzesińska et al., 2021)	hydrothermal processes and hydrothermal alteration or weathering of host rock	moderate (McIntosh et al., 2024)

(Continued on the following page)

TABLE 1 (*Continued*) Potential analogue rock samples present at Oxia Planum and their geological, paleoenvironmental, and biosignatures preservation potential.

Rock group	Rock type	Textural and morphological features to be captured with CLUPI	Analog sample origin/Information	Geological age and name of formation	Accessibility for further analysis	Previous observations on mars (examples)	Geological history and paleoenvironment	Biosignature preservation potential
B	Basaltic tuff (a) - Granby Tuff	Fe/Mg - phyllosilicates (smectite, vermiculite) - darkbrown clay minerals in vesicles (April and Keller, 1992; Robinson and Luttrell, 1985; Schlische, 1993; Krzesińska et al., 2021)	Granby Basaltic Tuff***	Late Triassic to Early Jurassic periods, roughly 200 to 220 Ma; olland Volcanic Series, which is associated with the Hartford Basin	Yes- via PTAL University of Oslo	Spectral signature of these terrestrial rocks match the mineralogy of Oxia Planum clays (OMEGA) (Krzesińska et al., 2021)	hydrothermal processes and hydrothermal alteration or weathering of host rock	moderate in vermiculite (McIntosh et al., 2024)
C	Basaltic tuff (b) - Granby Tuff	Fe/Mg - phyllosilicates (smectite, vermiculite) - darkbrown clay minerals in vesicles (April and Keller, 1992; Robinson and Luttrell, 1985; Schlische, 1993; Krzesińska et al., 2021)	Granby Basaltic Tuff***	Late Triassic to Early Jurassic periods, roughly 200 to 220 Ma; olland Volcanic Series, which is associated with the Hartford Basin	Yes- via PTAL University of Oslo	Spectral signature of these terrestrial rocks match the mineralogy of Oxia Planum clays (OMEGA) (Krzesińska et al., 2021)	hydrothermal processes and hydrothermal alteration or weathering of host rock	high - in vermiculite (McIntosh et al., 2024)
D	Vermiculitized chlorite-schists (Otago Schist)	Fe/Mg -phyllosilicates, green vermiculite and white kaolinite in the rock matrix (Craw et al., 1995; Krzesińska et al., 2021)	Otago, NZ***	middle to late Paleozoic era; 500–300 Ma; metamorphic formation	Yes- via PTAL University of Oslo	Spectral signature of these terrestrial rocks match the mineralogy of Oxia Planum clays (OMEGA) (Krzesińska et al., 2021)	low-grade metamorphism, low-temperature, weathering process, alteration of chlorite with groundwater to form clay minerals	high- in vermicullite (Mandon et al., 2021)
E	Conglomerate (Otago Schist Formation)	Fe/Mg -phyllosilicates, green vermiculite and white kaolinite in conglomerate clasts (Craw et al., 1995; Krzesińska et al., 2021)	Otago, NZ***	middle to late Paleozoic era; 500–300 Ma; metamorphic formation	Yes- via PTAL University of Oslo	Spectral signature of these terrestrial rocks match the mineralogy of Oxia Planum clays (OMEGA) (Krzesińska et al., 2021)	low-grade metamorphism, low-temperature, weathering process, alteration of chlorite with groundwater to form clay minerals (Craw et al., 1995; Krzesińska et al., 2021)	high- in vermicullite (Mandon et al., 2021)

(Continued on the following page)

10.3389/fspas.2025.1530408

TABLE 1 (*Continued*) Potential analogue rock samples present at Oxia Planum and their geological, paleoenvironmental, and biosignatures preservation potential.

Rock group	Rock type	Textural and morphological features to be captured with CLUPI	Analog sample origin/Information	Geological age and name of formation	Accessibility for further analysis	Previous observations on mars (examples)	Geological history and paleoenvironment	Biosignature preservation potential
F	Altered basalt	Fe/Mg -phyllosilicates - smectite, illite in the rock matrix, zeolites in the voids (Craw et al., 1995; Krzesińska et al., 2021)	Otago, NZ***	middle to late Paleozoic era; 500–300 Ma; metamorphic formation	Yes- via PTAL University of Oslo	Spectral signature of these terrestrial rocks match the mineralogy of Oxia Planum clays (OMEGA) (Krzesińska et al., 2021)	aleteration of basalts, precipitations of clay minerals (Craw et al., 1995; Krzesińska et al., 2021)	high - in vermicullite (Mandon et al., 2021)
3. Igneous rocks								
A	Picritic basalt	Olivine phenocrysts/porphyric texture	Unknown*	Unknown	Yes - via UniBasel	Curiosity and Perseverance rovers (McSween et al., 2006; Christensen et al., 2005)	one of the most common rock on Mars - volcanic activity/lava flows (McSween et al., 2006; Christensen et al., 2005)	none
B	Peridotite	Coarse-grained with oxides in the matrix	Unknown*	Unknown	Yes - via UniBasel	Found in olivine and pyroxene rich rocks on Mars, possibly peridotite (Mustard et al., 2005)	mantle processes, volcanic activty	none
C	Basalt	Presence of minerals (phenocrysts)	Eifel Volcanic Field, Germany*	Quaternary period; 500–10 Ma; Eifel Volcanic Group	Yes - via UniBasel	Curiosity and Perseverance rovers (McSween et al., 2006; Hamilton and Christensen, 2005)	volcanic activity/lava flows	none
D	Basalt	Vesicles, presence of minerals (phenocrysts)	Kaiserstuhl volcanic complex, Germany*	Miocene epoch - 16 to 11 Ma; Kaiserstuhl Formation	Yes - via UniBasel	Curiosity and Perseverance rovers (Crumpler et al., 2007; Joseph and Armstrong, 2022; Udry et al., 2023)	volcanic activity/explosive	moderate (in vesicles Cockell et al., 2019)
E	Basalt (lava)	Large vesicles, bubbles	Iceland**	Fagradalsfjall volcano eruption, 2021	Yes - via UniBern	Curiosity and Perseverance rovers (Crumpler et al., 2007; Joseph and Armstrong, 2022; Udry et al., 2023)	recent volcanic activity	none

(Continued on the following page)

TABLE 1 (*Continued*) Potential analogue rock samples present at Oxia Planum and their geological, paleoenvironmental, and biosignatures preservation potential.

Rock group	Rock type	Textural and morphological features to be captured with CLUPI	Analog sample origin/Information	Geological age and name of formation	Accessibility for further analysis	Previous observations on mars (examples)	Geological history and paleoenvironment	Biosignature preservation potential
F	Phonolite	Presence of minerals (phenocrysts)	Kaiserstuhl volcanic complex, Germany*	Miocene epoch - 16 to 11 Ma; Kaiserstuhl Formation	Yes - via UniBasel	Possibly Mars-analogue rock (Bost et al., 2013)	volcanic activity/explosive	none
4. Evaporites, carbonates and morphological biosginatures								
A	Jarosite in shale	Yellow mineral in the shale, kaolinite in the matrix (Martínez Frías et al., 2004)	Almeria, Spain***	Paleocene to Pliocene zone; Jaroso hydrothermal system (JHS)	Yes- via PTAL University of Oslo	Spirit, Opportunity and Curiosity rovers (Farrand et al., 2009; Elwood Madden et al., 2004; Fairén et al., 2009)	indication of past water activity, interaction of volcanic, evaporitic and hydrothermal processes	moderate (Farrand et al., 2009)
B	Jarosite in Ca and Ba sulphate deposit	Yellow mineral in Ca and Ba sulphate (Martínez Frías et al., 2004)	Almeria, Spain***	Paleocene to Pliocene zone; Jaroso hydrothermal system (JHS)	Yes- via PTAL University of Oslo	Spirit, Opportunity and Curiosity rovers (Farrand et al., 2009; Elwood Madden et al., 2004)	indication of past water activity, interaction of volcanic, evaporitic and hydrothermal processes	moderate (Farrand et al., 2009)
C	Carbonate	Deep cracks	Limestone from desert in Algier**	Unknown	Yes - via UniBern	e.g., found in Gusev Crater (Morris et al., 2010), in Jezero Crater (Clave et al., 2023), also with orbital observations (Ehlmann et al., 2008; Morris et al., 2010; Michalski and Niles, 2010)	typically indication of precipitation from seawater in shallow marine environment but also could result of a variety of processes including impact, igneous activity, weathering, and groundwater flow with diagenesis, good biosignature preservation potential	moderate (could biotic and abiotic)
D	Gypsum - e.g., veins or lenticular gypsum	Veins under the regolith (on Mars) or lenticular gypsum in modern evaporitic environment - high potential to trap and preserve microbes in fluid inclusions	modern gypsym from Dohat Faishakh Sabkha, Qatar	Middle Eocene, Upper Dam Formation; dolomitc limestone and marl member formaion (Braunger et al., 2018)	Yes - via UniBasel	Opportunity Rover (Squyers et al., 2012; Vaniman et al., 2018; Dilotero et al., 2023; Allwood et al., 2013)	evidence of water, evaporitic setting with a good biosignature preservation potential	high (Shkolyar and Farmer, 2018)

(Continued on the following page)

10.3389/fspas.2025.1530408

TABLE 1 (*Continued*) Potential analogue rock samples present at Oxia Planum and their geological, paleoenvironmental, and biosignatures preservation potential.

Rock group	Rock type	Textural and morphological features to be captured with CLUPI	Analog sample origin/Information	Geological age and name of formation	Accessibility for further analysis	Previous observations on mars (examples)	Geological history and paleoenvironment	Biosignature preservation potential
E	MISS in carbonates, Qatar	Fossilized, polygonal mats	Microbial mat, Al Majfar, Qatar	Quaternary, modern - 2,500–3,000 years old; sabkha deposits and marine calcareous sand	Yes - via UniBasel	Microbial mats not found on Mars, but polygonal structures found on Mars, although abiotic (Rapin et al., 2023)	potential to preserve microbes, evidence for evaporitic systems on Mars, life under extreme conditions/environment (Diloreto et al., 2023; Bontognali et al., 2020; El Maarry et al., 2010)	moderate (polygons could be also abiotic or related to water dry-wet cycles Rapin et al., 2023)
F	Stromatolite in chert (Pilbara) - stromatolitic laminations	Layers, stromatolitic texutre in chert	Pilbara, Australia	Archean, 3.5–3.4 Billion years, Dresser formation	Yes - via UniBasel	Not found on Mars yet- but a putative biosginature	could be a potential evidence of early life on Mars	high (Tewari, 1998; Allwood et al., 2007)
5. Rock with various morphological features								
A	Sediment with cracks	Dessication cracks/shrinkage cracks	Sedimentary cover, Thuringen Geopark, Germany	Middle Triassic, 247–243 Ma; Muschelkalk Formation; marine deposits	Yes- via UniBern	Mud cracks/butt cracks on Mars- Detected by Curiosity (abiotic) (Siebach et al., 2014) but on Earth could also be related to MISS (microbially induced sedimentary Structure)	fluvial erosion, aeolian processes, wet-dry cycles on Mars (Rapin et al., 2023)	moderate (could biotic and abiotic)
B	Sediment with erosional morphology	Rough wavy morphology	Natural Museum History at Bern (research collection)	Unknown	Yes- via UniBern	not detected - suggessted as potential MISS in clastic deposits by Noffke (2021)	indication of microbially induced sedimentary structures (MISS),fluvial or aeolian processes (Noffke, 2009; Noffke, 2021)	moderate (could biotic and abiotic)
C	Sediment with circular patterns (MISS)	Circular patterns	unknown sediment (sandstone + gravel) from Molasse basin, CH	Oligocene, 34 Ma; Central Moasse basin; marine deposit	Yes- via UniBern	not detected - suggessted as potential MISS in clastic deposits by Noffke (2021)	could be an indication of microbially induced sedimentary structures (MISS),fluvial, shallow water indication (Noffke, 2009; Noffke, 2021)	moderate (could biotic and abiotic)
D	Sediment with nodules	Sphere-shaped, clotted nodules	Natural Museum History at Bern (research collection)	Unknown	Yes- via UniBern	Opportunity and Spirit rovers " Martian blueberries" (Eberl, 2022)	indication of hematite, fluvial processes (acidic, liquid water) Eberl (2022)	moderate (could biotic and abiotic)

*UniBas research collection/**Natural History Museum Bern***PTAL, collection, University of Oslo Norway.

were likely in contact with water, producing hydrated alteration products (e.g., Poulet et al., 2005).

On Earth, two regions have been found to have matching spectral signatures of Fe-Mg phyllosilicates/hydrated clays with the ones detected by OMEGA in Oxia Planum (Krzesińska et al., 2021). These samples come from (1) vermiculated chlorite-schists from Otago, New Zealand, which underwent low-grade metamorphism, producing alteration of chlorite with groundwater to form clay minerals (Craw et al., 1995; Krzesińska et al., 2021; Mandon et al., 2021) and (2) basaltic tuffs from Granby, United States, with Fe-rich clays filling amygdales of supposedly hydrothermal origin (April and Keller, 1992; Schlische, 1993; Krzesińska et al., 2021). These rocks and features that should be observed with close-up cameras hosting Fe-Mg rich clays include altered and layered phonolites, vesicular/basaltic rock textures with clay minerals within the vesicles, fine-grained vermiculated chlorite schists with clay minerals within the rock matrix, and clay minerals precipitated within the conglomerate clasts of vermiculated schists (Krzesińska et al., 2021). Moreover, detecting vermiculite within the rock matrix, voids, and layers of altered igneous rocks would be crucial, as vermiculite has great potential to store organic matter (Krzesińska et al., 2021).

3.1.3 Igneous rocks

Igneous rocks dominate the Martian surface, particularly basalts (including picritic basalt and trachybasalts) and peridotites (McSween et al., 2006). These rocks have been detected by current active rovers e.g., Curiosity and Perseverance (e.g., Christensen et al., 2005; Hamilton and Christensen, 2005; Crumpler et al., 2007; Joseph and Armstrong, 2022; Liu et al., 2022; Udry et al., 2023; Grotzinger et al., 2013), and their study provided insight into Mars' geological history, mantle processes, and volcanic activity. Despite their abundant occurrence and geological relevance, they provide a challenging environment for habitability and are not considered a prime target for searching for biosignatures. Nevertheless, it remains important to study their textures, phenocrysts, vesicles, and mineralogy to unravel the past of Oxia Planum, including potential volcanic eruptions and the interaction of igneous rocks with ancient aqueous environments. To study the volcanic history within Oxia Planum, collecting basaltic rocks will be possible within the old volcanic unit (Vc) and the much younger Amazonian dark-resistant unit (Adru) to confirm the origin of its formation and the role of the mafic unit in protecting the underlying phyllosilicate unit from cosmic radiation (e.g., Kminek and Bada, 2006; Vago et al., 2017).

3.1.4 Evaporites, carbonates and morphological biosignatures

Another set of highly interesting sample targets includes rocks formed through direct precipitation from liquid water, such as carbonates, sulphates (including jarosite), and gypsum, making them proxies for past aqueous activity (Squyres et al., 2012; Nachon et al., 2014). Additionally, carbonates and evaporites are often associated to both morphological and geochemical biosignatures (Schreiber et al., 2001). For example, stromatolites interpreted as fossil microbialites (Allwood et al., 2007) are often comprised of carbonate minerals and, in rare occurrences, they can also preserve remains of the biomass of ancient microbial mats (Bontognali et al., 2012). Although stromatolites have not yet been detected on Mars, the search for stromatolite-like morphologies should be considered while exploring Oxia Planum, as on Earth, these rocks are present in formations of similar age and represent some of the earliest evidence of life (Awramik, 1992).

Similarly, to carbonates, also gypsum it is considered a promising mineral where to look for both fossil organisms (Schopf et al., 2012) and biomarkers (DiLoreto et al., 2023). While there is no conclusive evidence based or spectral analysis acquired with orbiters about the presence of carbonates and sulphates at Oxia Planum, these minerals have been found in other regions of Mars with geological settings and units like Oxia Planum. For example, carbonates were detected in Gusev crater by e.g., Morris et al. (2010). Carbonates were also detected by the Mars Reconnaissance Orbiter in the Nili Fossae region, associated with both phyllosilicate-bearing and olivine-rich rocks from the Noachian period (Ehlmann et al., 2008), and later within Jezero crater (Clave et al., 2023).

Another mineral found on Mars that forms exclusively in association with water and serves as strong evidence of past aqueous activity is jarosite, a yellow mineral precipitated within the rock matrix in sulphates or shales (Farrand et al., 2009; Elwood Madden et al., 2004). Gypsum, which was also identified on Mars by the Opportunity rover as a bright vein mineral deposited by water Squyres et al., 2012), is another crucial target. Moreover, all these rock types have the potential to be found across the entirety of Oxia Planum, especially in association with clay/Fe-Mg phyllosilicate minerals. Additionally, they possess excellent potential for preserving biosignatures within their textures, mineral compositions, and even within fluid inclusions (e.g., within gypsum; Gill et al., 2023). Therefore, the search for these rock types should also be a priority for astrobiological sampling.

3.1.5 Rocks with various morphological features

In this last category, we include rocks characterized by morphological features that cannot always be unequivocally attributed to primary processes vs. diagenetic/metamorphic processes vs. late-stage erosion and weathering processes (e.g., Mustoe, 1982; Mustoe, 2010). Indeed, microbe-mineral interactions create primary sedimentary structures (e.g., stromatolites, MISS (Noffke, 2010), which, especially in very old outcrops, are sometimes difficult to differentiate from late-stage secondary structures resulting from erosion processes caused by wind, water, or ice. For example, cracks and erosional morphologies may arise from aeolian weathering, abrasion, thermal stress, or they could be remnants of MISS, particularly when displaying circular, sphere-shaped, polygonal, ripple-like, and hydraulic patterns within the host sediments (Noffke, 2009; El Maarry et al., 2010; Guerrero and De Wit, 1992). Confirming their biogenic origin necessitates consideration of additional factors, including geological context, mineralogical characteristics, and geochemical signatures. Similarly, diagenetic processes, such as compaction and cementation, contribute to the formation of concretions and nodules (e.g., Raiswell, 1987; Seilacher, 2001). Further modifications occur through hydrothermal and chemical alteration, where mineral precipitation from fluid interactions leads to the development of veins (Meunier, 1995; Schwenzer et al., 2016). On Mars such features were previously documented including, for example, hematite-rich nodules, commonly known as "Martian blueberries" (Eberl, 2022). These nodules are hypothesized to have formed either as sediment concentrations from hydrothermal solutions following a bolide impact into groundwater or permafrost, or through the precipitation of minerals from water circulating through porous rocks. Their presence highlights the intricate relationship between geological and hydrological processes on the Martian surface. Other nodules observed include diagenetic nodules (Stack et al., 2014) and Manganese-iron phosphate nodules in Gale crater (Treiman et al., 2023). All these rock facies rich in morphological features could also be interesting to capture with CLUPI and later analysed by the rover for further study.

4 Results

4.1 An image catalogue of rock textures and morphological biosignatures in Oxia Planum

We compiled an image catalogue consisting of five figures (Figures 3–7), showcasing CLUPI's capability to capture rock textures and sedimentary structures relevant to the ExoMars mission. The first picture always provides an overview of the sample, with all pictures having FOV 2, measuring 10.4 × 4.4 cm and with a resolution of 2,652 × 1,128 pixels. The square pictures are close-up sections of the original image, highlighting the texture or morphology of interest. The left square rock texture was photographed under diffused light conditions only, the middle square represents mid-day conditions, and the right square represents evening/morning conditions.

4.1.1 Clastic sedimentary rocks

As representative sedimentary rocks (Figure 3), we selected the samples that were identified in several areas of Mars during previous missions (section 3.1.1). These include sandstones with various grain sizes: coarse-grained, equigranular sandstone (0.5 mm) with laminations (Figure 3A), coarse-grained sandstone (0.25–0.5 mm) (Figures 3A1), fine-grained sandstone (0.1–0.25 mm) (Figures 3A2), very fine-grained sandstone (0.06–0.1 mm) (Figures 3A3), feldspar-rich sandstone (Figure 3B), conglomerate with sub-rounded grains (Figure 3C), mudstone with fine laminations (Figure 3D), and mudstone with laminations (E).

To identify sedimentary laminations, particularly the finer ones with widths of 0.1 mm (Figures 3D,E), a 25° solar angle, corresponding to morning or evening conditions, is the most suitable. These lighting conditions create prominent shadows, accentuating the rock surface morphology and highlighting some of the finest laminations that are poorly visible under diffused light or a higher solar angle (70°).

For Sample B (feldspar-rich sandstone), where grain sizes range from 0.1 to 2 mm, diffused lighting is the most effective in revealing its poorly sorted texture with angular grains. Also, to accurately capture features such as grain size, shape, and orientation (Figures 3A–C), diffused light is preferred. This lighting condition minimizes shadows, enhancing the visibility of these features while reducing colour saturation, which facilitates the detailed observations of even the smallest pebbles. This finding is further supported by observations from Sample 3A, where laminations in sandstone (0.1 cm width) are attributed to colour variations caused by mineralogical or compositional differences. For both Sample 3A and the conglomerate (3B), diffused light provides superior results compared to a 70° solar angle, with the 25° angle being the least effective.

Our results show that CLUPI, at a 50 cm working distance, can easily identify fine-to coarse-grained, equigranular, well-sorted sandstone with grain sizes ranging from 0.1 to 0.5 mm (Figures 3A–A2). The very fine-grained sandstone (Figures 3A3, 0.06–0.1 mm) represents the resolution limit at which CLUPI can still distinguish individual grains. Therefore, the visibility of granulometry and texture is primarily determined by resolution rather than lighting conditions. In contrast, PanCam's Wide-Angle Camera (WAC), typically operating at a working distance of ~2–3 m, lacks the resolution to resolve grains smaller than 0.25 mm (Coates et al., 2017). The High-Resolution Camera (HRC), at a working distance of ~2 m, has a best resolution of ~0.17 mm/pixel, meaning it can only detect grains larger than ~0.15 mm. As a result, grains finer than 0.1 mm would appear as homogeneous textures in PanCam images rather than individually resolved particles, highlighting CLUPI's advantage in distinguishing fine-grained sediments.

4.1.2 Rocks with Fe-Mg phyllosilicates

As representative Fe-Mg phyllosilicate rocks (Figure 4) we selected terrestrial mineralogical equivalents (section 3.1.2) of Oxia Planum phyllosilicates (Krzesińska et al., 2021). The mineralogical composition of these samples has been determined through analysis conducted by the PTAL group at the University of Oslo. However, during the mission, colour alone will not serve as a reliable indicator of mineral composition but rather as an indicator of interesting heterogeneities in rock texture. These heterogeneities warrant further analysis using other spectrometers to confirm mineralogical identification.

The samples used in our study are A–altered phonolite with Fe/Mg phyllosilicates, B- basaltic tuff (a) with dark brown Fe-Mg phyllosilicates in vesicles, C - basaltic tuff (b) with dark brown Fe-Mg phyllosilicates in vesicles, D–Vermiculite chlorite-schist with green vermiculite and white kaolinite, E– Conglomerate with green vermiculite and white kaolinite, F- altered basalt with clays in the matrix and voids. This set of rocks is characterized by the importance of detecting not just the morphology and textures of rocks, but also the areas of interest where the phyllosilicate minerals can be identified, such as fine laminations (Figure 4A) or vesicles with a diameter of ~0.2 cm (Figures 4B,C,F).

Our results indicate that diffuse lighting is generally preferred for detecting small textural and colour differences (Figures 4D,E) associated with phyllosilicate minerals, thereby enhancing their visibility within rock textures. However, at a low angle of 25°, the strong shadowing effect inhibits the identification of phyllosilicates within the host rock.

4.1.3 Igneous rocks

As representative igneous rocks (Figure 5), we selected rocks that were identified in several areas of Mars during previous missions (section 3.1.3): A–picritic basalt with olivine phenocrysts, B–peridotite with oxides, C–basalt with phenocrysts, D–vesicular

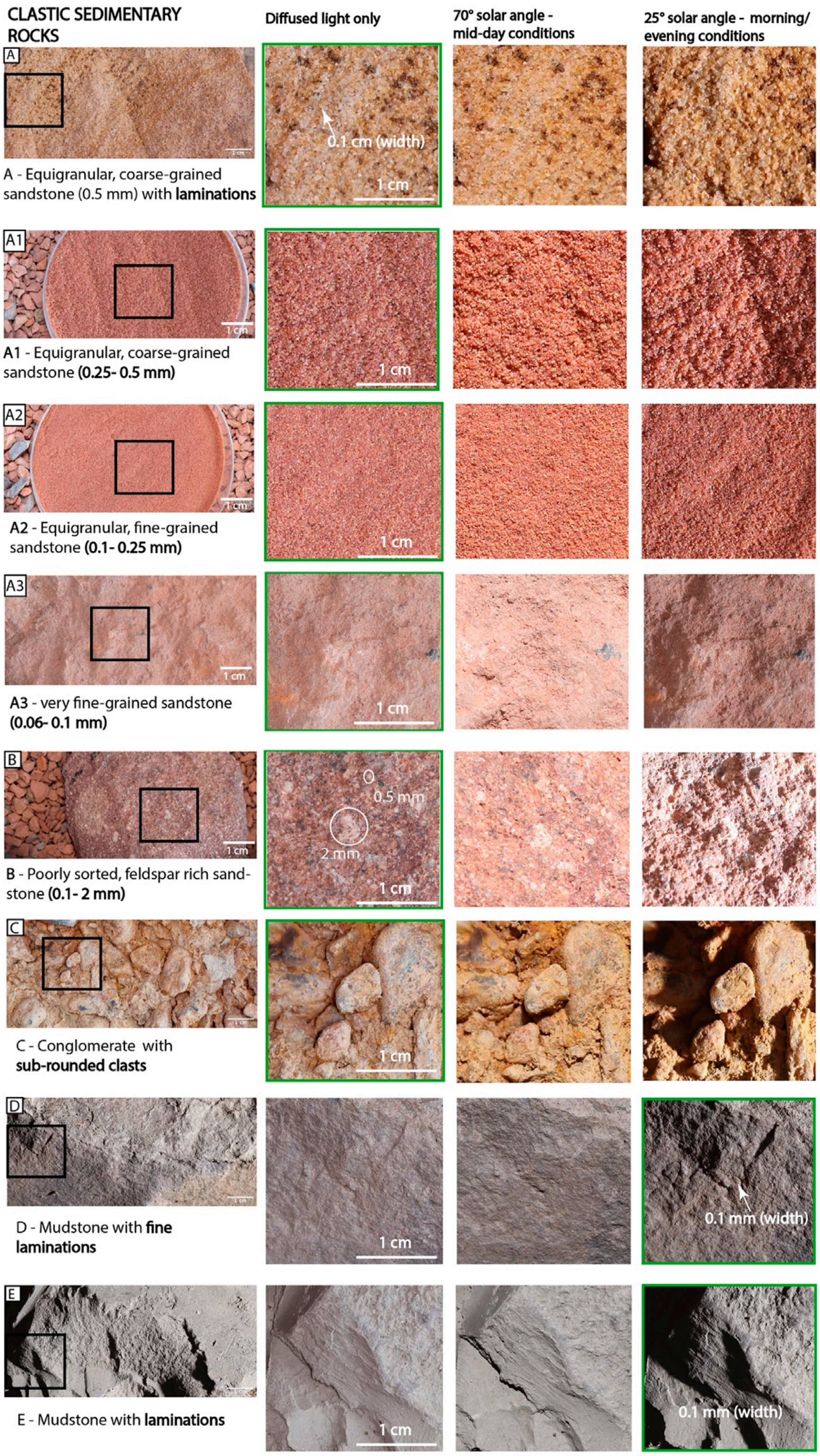

FIGURE 3
Clastic sedimentary rocks and their textures photographed with CLUPI analogue camera under three variable lighting conditions, where the green box indicates the most preferred conditions. **(A)** - Equigranular, coarse-grained sandstone (0.5 mm) with laminations; **(A1)** - Equigranular, coarse-grained sandstone (0.25 - 0.5 mm); **(A2)** - Equigranular, fine-grained sandstone (0.1 - 0.25 mm); **(A3)** - Very fine-grained sandstone (0.06 - 0.1 mm).; **(B)** - Poorly sorted, feldspar rich sandstone (0.1 - 2 mm); **(C)** - Conglomerate with sub-rounded clasts; **(D)** - Mudstone with fine laminations; **(E)** - Mudstone with laminations. For mid-day conditions, all images were acquired with 1,000 lux of diffused light and 5,000 lux of direct plus diffused light. The illumination axis had a polar angle of 20° and an azimuthal angle of 90° (i.e., illumination perpendicular to the target surface), while the optical axis had a polar angle of 78.5° and an azimuthal angle of 270°. For morning/evening conditions, all images were acquired with 1,000 lux of diffused light and 5,000 lux of direct plus diffused light. The optical axis maintained a polar angle of 78.5° and an azimuthal angle of 270°, while the illumination axis had a polar angle of 65° and an azimuthal angle of 180° (i.e., illumination perpendicular to the target surface). For all diffused light images, only 1,000 lux of diffused light was applied; hence, there was no illumination axis, and the optical axis maintained a polar angle of 78.5° and an azimuthal angle of 270°.

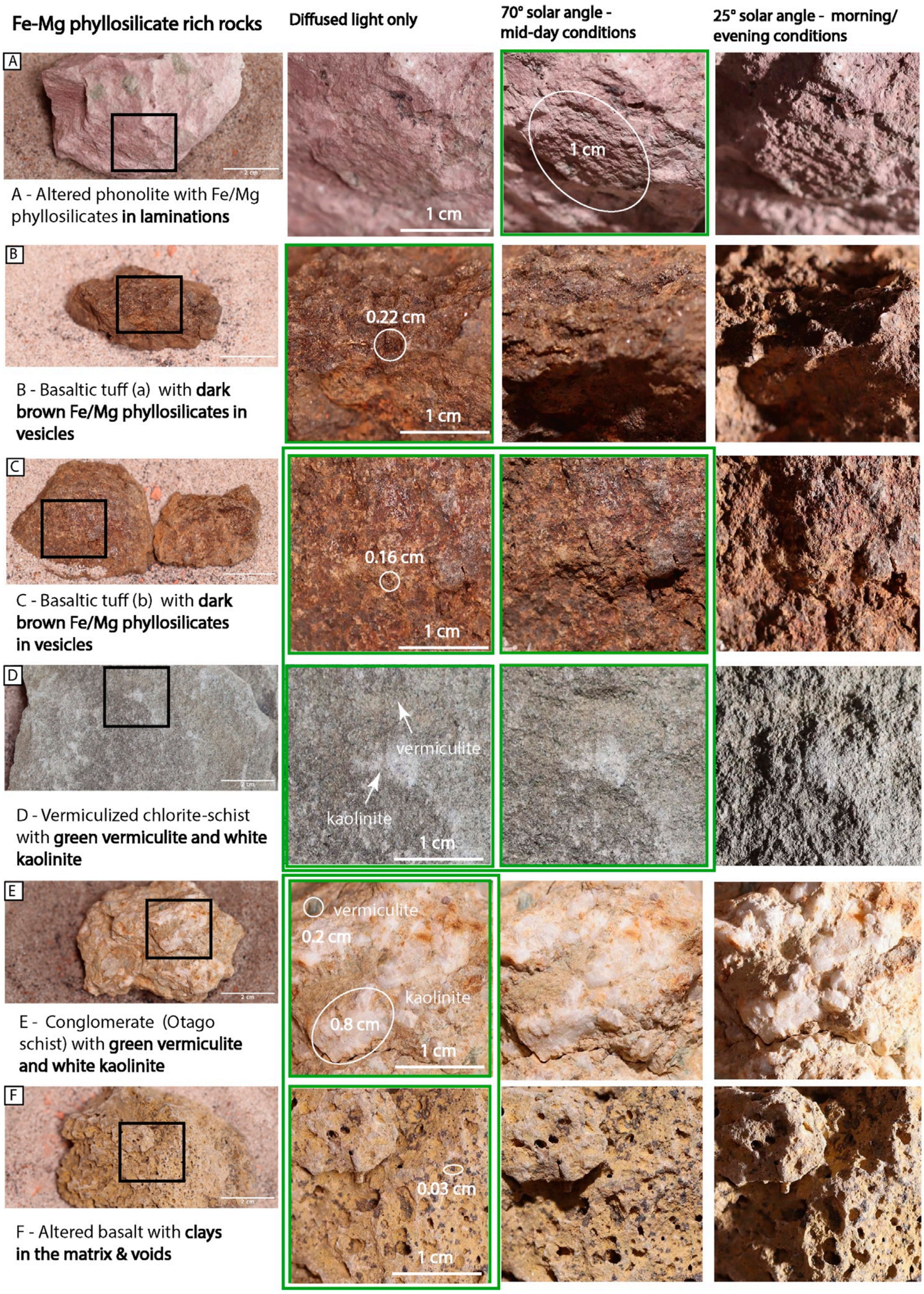

FIGURE 4
Fe-Mg phyllosilicates and their textures photographed with CLUPI analogue camera under three variable lighting conditions, where the green box indicates the most preferred conditions. **(A)** - Altered phonolite with Fe/Mg phyllosilicates in laminations; **(B)** - Basaltic tuff (a) with dark brown Fe/Mg phyllosilicates in vesicles; **(C)** - Basaltic tuff (b) with dark brown Fe/Mg phyllosilicates in vesicles; **(D)** - Vermiculized chlorite-schist with green vermiculite and white kaolinite; **(E)** - Conglomerate (Otago Schist) with green vermiculite and white kaolinite; **(F)** -Altered basalt with clays in the matrix & voids. For mid-day conditions, all images were acquired with 1,000 lux of diffused light and 5,000 lux of direct plus diffused light. The illumination axis had a polar angle of 20° and an azimuthal angle of 90° (i.e., illumination perpendicular to the target surface), while the optical axis had a polar angle of 78.5° and an azimuthal angle of 270°. For morning/evening conditions, all images were acquired with 1,000 lux of diffused light and 5,000 lux of direct plus diffused light. The optical axis maintained a polar angle of 78.5° and an azimuthal angle of 270°, while the illumination axis had a polar angle of 65° and an azimuthal angle of 180° (i.e., illumination perpendicular to the target surface). For all diffused light images, only 1,000 lux of diffused light was applied; hence, there was no illumination axis, and the optical axis maintained a polar angle of 78.5° and an azimuthal angle of 270°.

basalt with phenocrysts and vesicles, E–basalt (lava) with large vesicles/bubbles, F- phonolite with diverse phenocrysts. For this group, the most relevant texture to be identified is the presence or absence of different sizes and shapes of phenocrysts or vesicles (Figure 5E). Our results provide evidence that such features are extremely challenging to identify with the lower solar angle of 25°, especially for small phenocrysts and oxide minerals in samples Figure 5B (size: 0.02–0.8 mm), Figure 5C (size: 0.7 mm-0.3 cm), and for sample Figure 5F (size: ~0.06 cm) where it is difficult to clearly distinguish between different types of phenocrysts. In contrast, the higher solar angle of 70° is the most preferred for recognising such features within the rock, as it minimises shadowing on the rock surface and reveals even the smallest minerals (Figures 5A,B).

4.1.4 Evaporites, carbonates and morphological biosignatures

In the group of evaporites, carbonates and morphological biosignatures (Figure 6), we identified (section 3.1.4): A-(yellow/orange) jarosite in shale, B – (yellow/orange) jarosite in Ca & Ba sulphate deposit, C–Carbonate, D–Gypsum, E– MISS in carbonates, Qatar, and F–stromatolite.

For prominent morphologies, such as stromatolitic laminae (0.7–1 cm wide) in stromatolite (Figure 6F) and MISS in carbonates (Qatar, Figure 6E), there appears to be no significant difference in preferred lighting conditions, as these features are distinct enough to be captured even under challenging lighting. However, different lighting highlights specific characteristics of these features. For instance, in Figure 6F, stromatolitic laminae and their colour heterogeneities are more apparent under diffused and midday lighting, whereas low-angle light better emphasises the sample's topography. For MISS in carbonates (Figure 6E), the morphology is visible in all lighting conditions, but low-angle light can create pronounced shadows due to the uneven topography, potentially obscuring the recognition of the rock matrix.

When capturing fine hydrothermal minerals within the rock texture, such as jarosite within sulphate (Figures 6A,B), carbonate textures (Figure 6C), or gypsum veins in the regolith (Figure 6D), diffused light with the lowest contrast is preferred. This lighting minimises shadows, enhancing the visibility of these minerals and textures, similar to the case of Fe-Mg phyllosilicates (Figure 4).

4.1.5 Rocks with various morphological features

The last group consists of samples with various morphological features (section 3.1.5) (Figure 7): A–sediment with cracks, B-sediment with erosional morphology, C- sediment with circular patterns (potential MISS) and D-sediment with nodules. Similarly, to MISS (Figure 6E) and stromatolites (Figure 6F), all these samples have a distinct and prominent morphologies making them possible to identify in each lighting conditions. The morphologies of samples Figures 7A–C are even more highlighted with a contrasting light of 25° of solar angle. However, to better study the matrix of the rock (Figure 7D), the light with less contrast (70° solar angle) is the most preferred to capture even the smallest details within the structures, e.g., spherules with ~0.5 cm.

4.2 Image analysis - sedimentary vs igneous rock textures under variable illumination

After compiling an image catalogue and investigating the impact of different illumination conditions on the recognition of specific features in Oxia Planum analogue rocks, we conducted a quantitative analysis on four of the most common and highly contrasting samples likely to be encountered during the ExoMars operations (see Supplementary Figure S2). It should be noted that these results are specific to the samples chosen for the simulations. The values obtained with this quantitative approach are expected to vary depending on the sample analysed, due to factors such as differences in sample morphology and surface flatness or unevenness and should be understood only as additional confirmation of the qualitative conclusions that can be drawn by visual interpretation of the figures.

All image analyses were performed using ImageJ software, after converting all images of interest to greyscale 8-bit format (0–255). We analysed regions of interest (ROIs) for both 70° midday and 25° evening/morning light conditions (Figure 8). For Sample A: Basalt with large phenocrysts (3 mm in size) – porphyritic texture, we manually outlined phenocrysts and their surrounding matrix for ten samples. For Sample B: Phonolite with diverse phenocrysts (average 1 mm in size) – phaneritic texture, we outlined ten black and ten white phenocrysts. For Sample C: Mudstone with fine laminations (0.2 mm width) and Sample D: Pilbara stromatolite with fine laminae (0.5 mm width), we drew a transect (or line) through the regions of interest. For Sample C, the transect spanned 1–69 pixels under both lighting conditions. For Sample D, the transect spanned 1–91 pixels for midday light and 1–105 pixels for morning/evening light.

For each highlighted feature, we calculated the mean brightness (0–255), standard deviation (StdDev), and mode, representing the most frequent pixel value within the ROI. Additionally, T-tests were performed to assess the statistical significance of the analysed datasets. All calculated values for each group are provided in the (Supplementary Table S1, S2).

Figure 8 summarises the impact of variable illumination conditions on the recognition of features within sedimentary and igneous rocks.

For Sample A: Basalt with large phenocrysts (3 mm in size) – porphyritic texture, under midday light, the mean brightness for phenocrysts is 87.2, while for the surrounding matrix it is 125.7. The negative t-statistic (−11.60) suggests that the matrix group has a significantly higher mean brightness than the phenocrysts group. The p-value (9.06×10^{-9}) is extremely low ($p < 0.001$), confirming high statistical significance between the phenocryst and matrix groups. This indicates that the observed difference is unlikely to be due to random variation. Under evening/morning light, the mean brightness for phenocrysts is 52.3, while for the surrounding matrix it is 104.6, reflecting an overall lower brightness compared to midday conditions. The negative t-statistic (−2.95) again suggests that the matrix group has a significantly higher mean brightness than the phenocrysts group. The p-value (0.0113) is below 0.05,

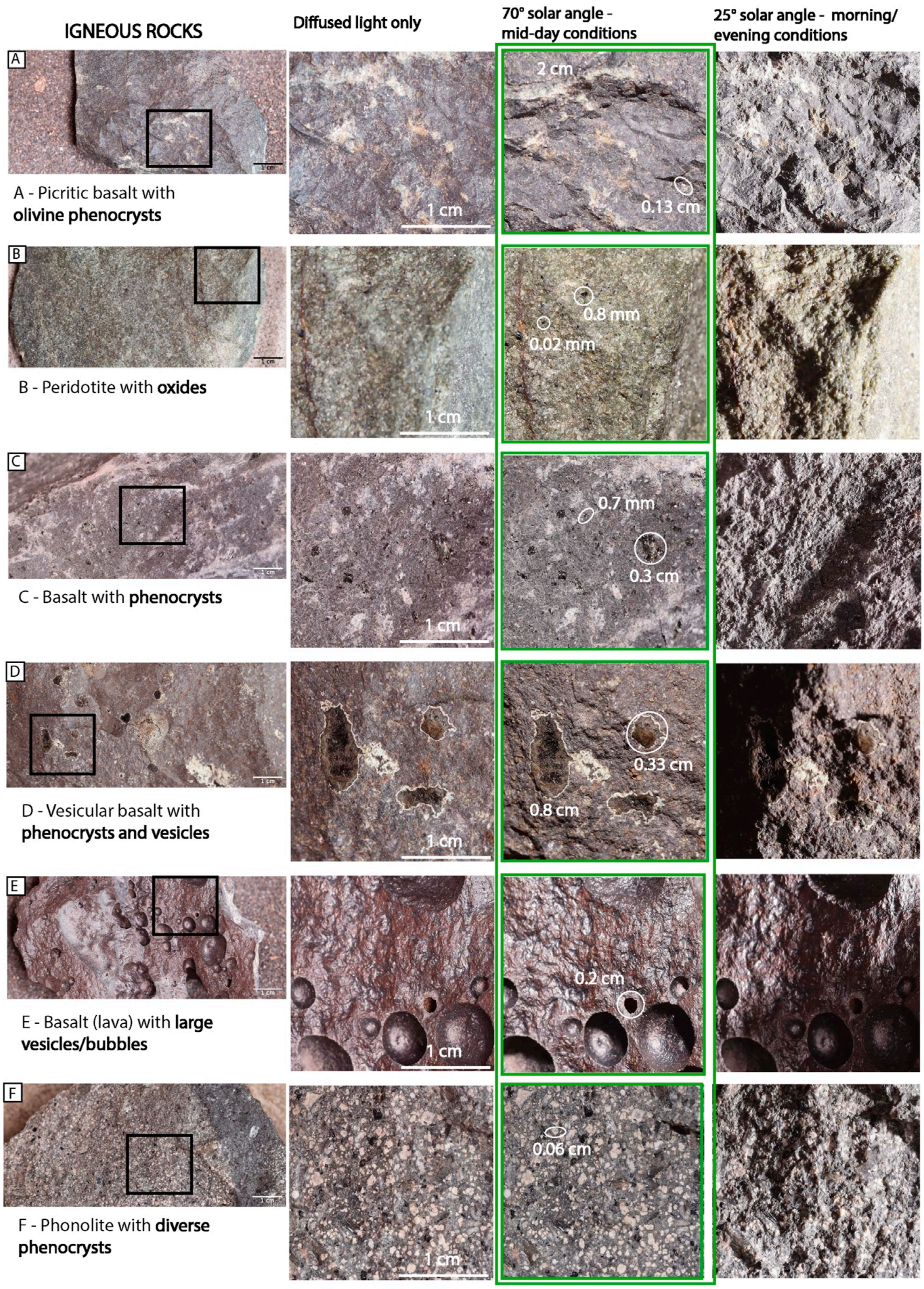

FIGURE 5
Igneous rocks and their textures photographed with CLUPI analogue camera under three variable lighting conditions, where the green box indicates the most preferred conditions. **(A)** - Picritic basalt with olivine phenocrysts; **(B)** - Peridotite with oxides; **(C)** - Basalt with phenocrysts; **(D)** - Vermiculized basalt with phenocrysts and vesicles; **(E)** - Basalt (lava) with large vesicles/bubbles; **(F)** - Phonolite with diverse phenocrysts. For mid-day conditions, all images were acquired with 1,000 lux of diffused light and 5,000 lux of direct plus diffused light. The illumination axis had a polar angle of 20° and an azimuthal angle of 90° (i.e., illumination perpendicular to the target surface), while the optical axis had a polar angle of 78.5° and an azimuthal angle of 270°. For morning/evening conditions, all images were acquired with 1,000 lux of diffused light and 5,000 lux of direct plus diffused light. The optical axis maintained a polar angle of 78.5° and an azimuthal angle of 270°, while the illumination axis had a polar angle of 65° and an azimuthal angle of 180° (i.e., illumination perpendicular to the target surface). For all diffused light images, only 1,000 lux of diffused light was applied; hence, there was no illumination axis, and the optical axis maintained a polar angle of 78.5° and an azimuthal angle of 270°.

10.3389/fspas.2025.1530408

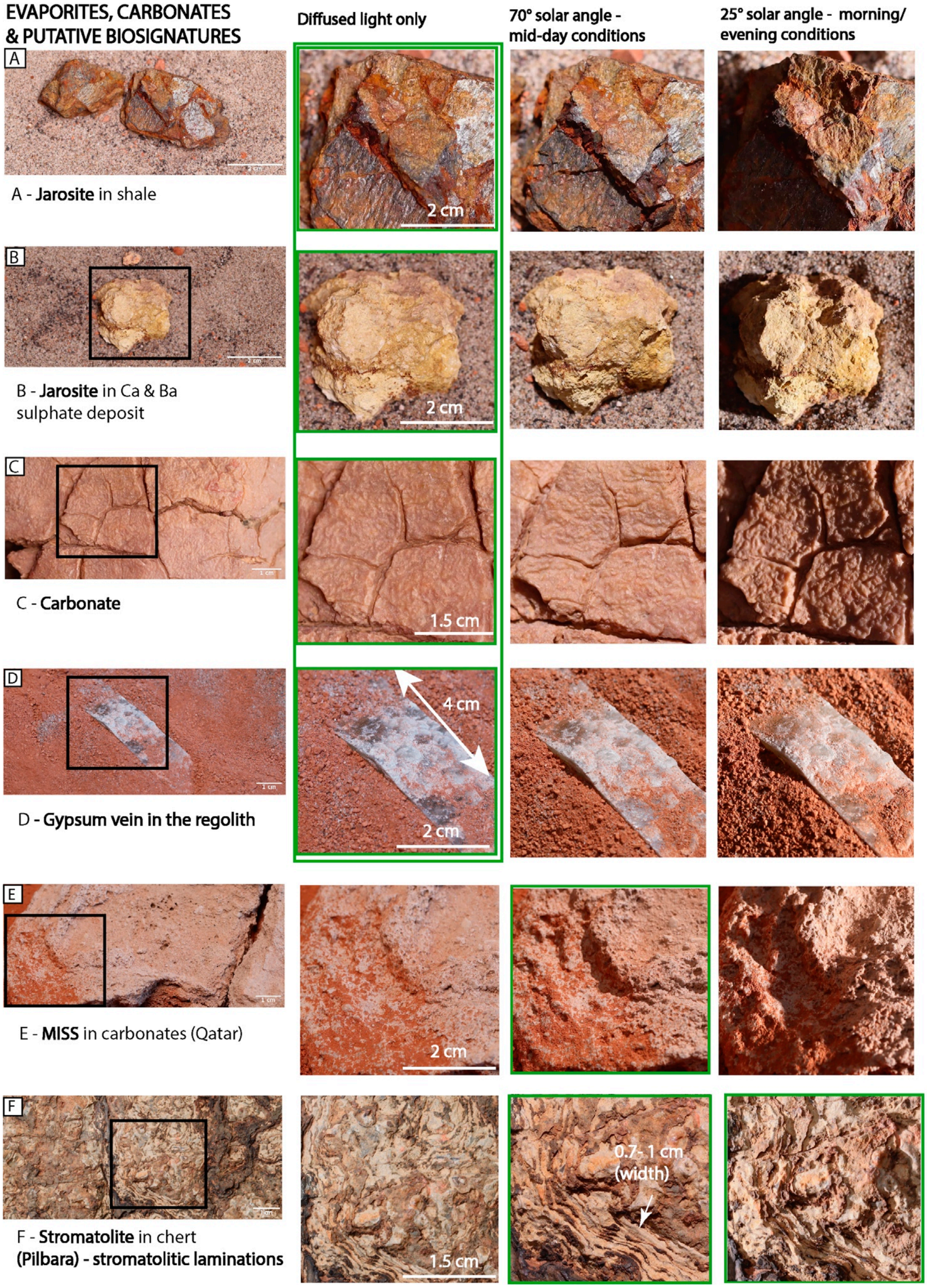

FIGURE 6
Evaporites, carbonates & putative biosignatures and their textures photographed with CLUPI analogue camera under three variable lighting conditions, where the green box indicates the most preferred conditions. **(A)** - Jarosite in shale; **(B)** - Jarosite in Ca & Ba sulphate deposit; **(C)** - Carbonate; **(D)** - Gypsum vein in the regolith; **(E)** - MISS in carbonates (Qatar); **(F)** - Stromatolite in chert (Pilbara) - stromatolitic laminations. For mid-day conditions, all images were acquired with 1,000 lux of diffused light and 5,000 lux of direct plus diffused light. The illumination axis had a polar angle of 20° and an azimuthal angle of 90° (i.e., illumination perpendicular to the target surface), while the optical axis had a polar angle of 78.5° and an azimuthal angle of 270°. For morning/evening conditions, all images were acquired with 1,000 lux of diffused light and 5,000 lux of direct plus diffused light. The optical axis maintained a polar angle of 78.5° and an azimuthal angle of 270°, while the illumination axis had a polar angle of 65° and an azimuthal angle of 180° (i.e., illumination perpendicular to the target surface). For all diffused light images, only 1,000 lux of diffused light was applied; hence, there was no illumination axis, and the optical axis maintained a polar angle of 78.5° and an azimuthal angle of 270°.

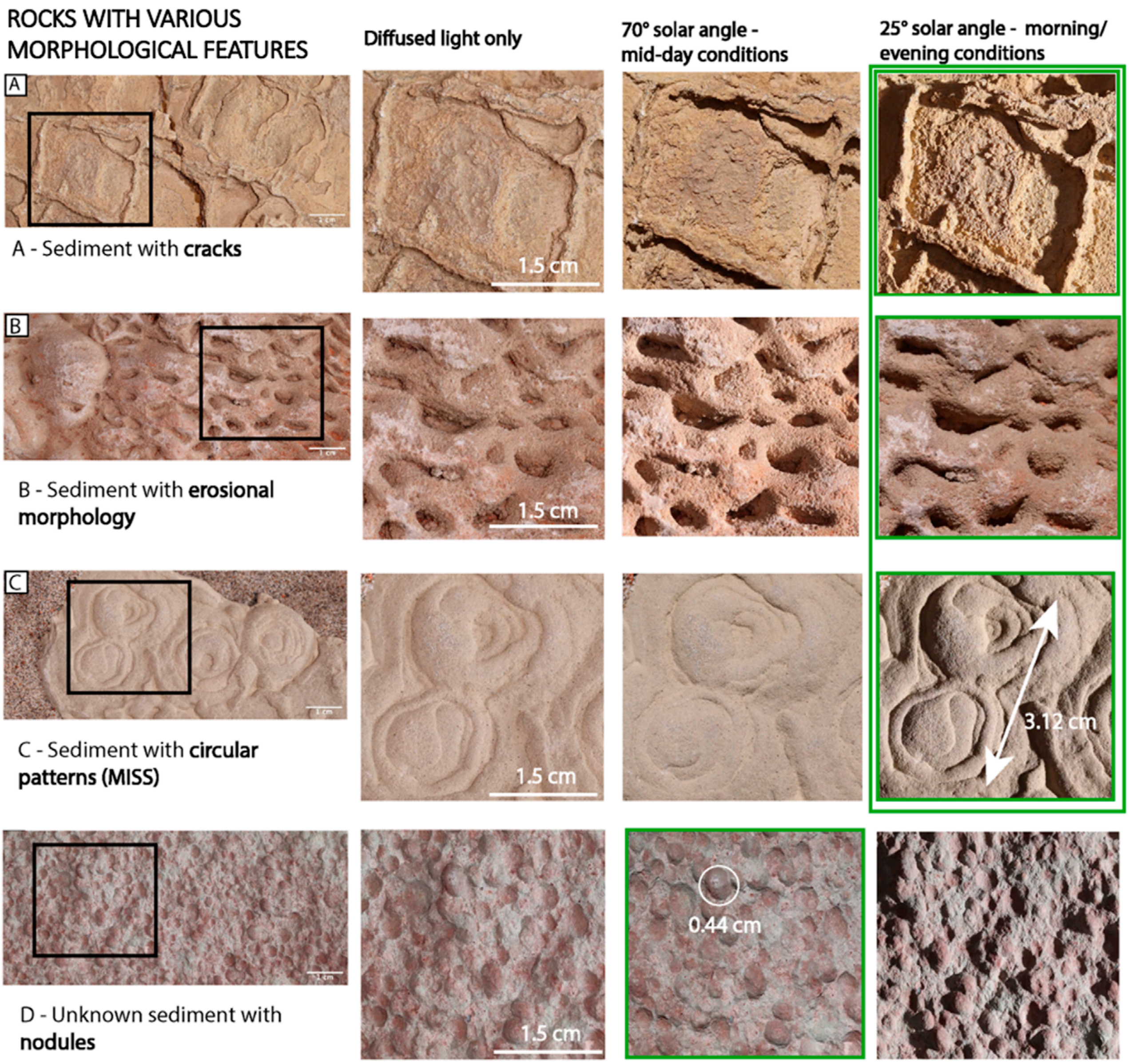

FIGURE 7
Rocks with various morphological features photographed with CLUPI analogue camera under three variable lighting conditions, where the green box indicates the most preferred conditions. **(A)** - Sediment with cracks; **(B)** - Sediment with erosional morphology; **(C)** - Sediment with circular patterns (MISS); **(D)** - Unknown sediment with nodules. For mid-day conditions, all images were acquired with 1,000 lux of diffused light and 5,000 lux of direct plus diffused light. The illumination axis had a polar angle of 20° and an azimuthal angle of 90° (i.e., illumination perpendicular to the target surface), while the optical axis had a polar angle of 78.5° and an azimuthal angle of 270°. For morning/evening conditions, all images were acquired with 1,000 lux of diffused light and 5,000 lux of direct plus diffused light. The optical axis maintained a polar angle of 78.5° and an azimuthal angle of 270°, while the illumination axis had a polar angle of 65° and an azimuthal angle of 180° (i.e., illumination perpendicular to the target surface). For all diffused light images, only 1,000 lux of diffused light was applied; hence, there was no illumination axis, and the optical axis maintained a polar angle of 78.5° and an azimuthal angle of 270°.

indicating a statistically significant difference, though smaller than under midday light.

For Sample B: Phonolite with diverse phenocrysts (average 1 mm in size) – phaneritic texture, under midday light, the mean brightness for white phenocrysts is 184, while for black phenocrysts it is 66. The large positive t-statistic (21.51) indicates that the white phenocrysts have significantly higher brightness than the black phenocrysts. The p-value (2.04×10^{-13}) is extremely low, confirming a highly significant difference between the two groups. Under evening/morning light, the mean brightness for white phenocrysts is 159, while for black phenocrysts it is 55, again indicating an overall lower brightness compared to midday conditions.

For identifying phenocrysts in the igneous rock sample (Sample A), the high 70° midday solar angle is preferred. Although both lighting conditions (midday and evening/morning) are statistically significant ($p < 0.05$), the p-value is significantly smaller for

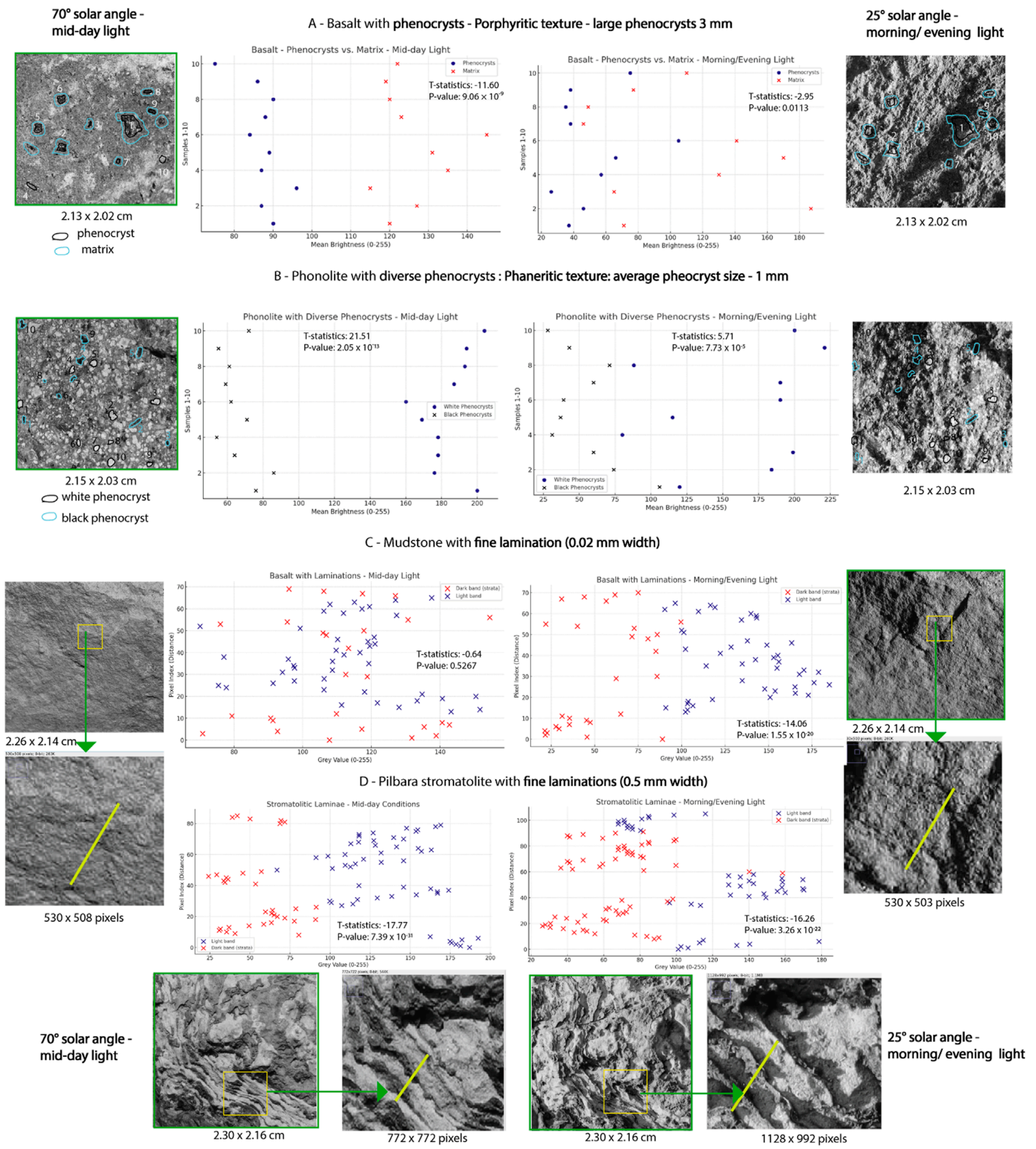

FIGURE 8
Mid-day and evening/morning light conditions and their impact on identifying and analysing morphological features of Oxia Planum analogue rocks.

midday conditions (9.06×10^{-9}) compared to evening/morning conditions (0.0113).

Examining the standard deviation (StdDev) values (Supplementary Table S1) reveals that under midday conditions, the phenocrysts group exhibited significantly higher contrast relative to the matrix, whereas in evening/morning conditions, the contrast between phenocrysts and matrix was much lower. Additionally, the difference in brightness was more pronounced under midday conditions, as indicated by the lower p-value, which signifies a stronger statistical difference.

This result can be attributed to the fact that certain phenocrysts and areas of the matrix in evening/morning light are significantly darker (e.g., phenocryst 1, with a mean brightness of 90 in midday light and 37 in evening/morning light), which are masked by shadows created by the low-angle light. This reduced contrast makes them more difficult to identify under evening/morning conditions. Conversely, some phenocrysts, such as phenocryst 6, appear overexposed in evening/morning light, with a mean brightness of 105 compared to 84 in midday conditions. These findings demonstrate that the p-values are lower for midday light, favouring these lighting conditions for distinguishing phenocrysts from the matrix more effectively.

In Sample B, the high 70° midday solar angle is also preferred for identifying white and black phenocrysts. The p-value is small (below 0.05) for both lighting conditions. However, the t-statistic for standard deviation (0.78; see Supplementary Table S1) indicates minimal contrast difference between white and black phenocrysts under evening/morning light. Under evening/morning light, some phenocrysts are obscured by shadows. For example, white phenocryst 4 had a mean brightness of 178 under midday light but only 80 under evening/morning light, making it more challenging to distinguish from black phenocrysts. Therefore, midday conditions, with reduced shadowing and enhanced contrast on the rock surface, are more effective for identification of black phenocrysts. The p-value (7.73×10^{-5}) remains extremely small, indicating a highly significant difference.

For Sample C: Mudstone with fine laminations (0.2 mm width), under midday light, the mean brightness for the dark band (strata) is 111, while for the light band it is 112. The negative t-statistic (−0.64) indicates that the difference in mean brightness between dark and light bands is not statistically significant. The p-value (0.5267) is much greater than the significance threshold of 0.05, meaning the observed difference can be attributed to random variability rather than a meaningful difference. Under evening/morning light, the mean brightness for the dark band is 50, while for the light band it is 128, showing a stark contrast compared to midday conditions. The negative t-statistic (−14.06) indicates that the light bands have significantly higher mean brightness than the dark bands. The p-value (1.55×10^{-20}) is extremely low, confirming a highly significant difference between the two groups.

For Sample D: Pilbara stromatolite with fine laminae (0.5 mm width), under midday light, the mean brightness for the dark band (strata) is 56, while for the light band it is 142. The negative t-statistic (−17.77) indicates that the light bands have a significantly higher mean brightness than the dark bands. The p-value (7.39×10^{-31}) is extremely low, confirming a highly significant difference between the two groups. Under evening/morning light, the mean brightness for the dark band is 75, while for the light band it is 142, which is comparable to midday conditions. The negative t-statistic (−16.25) indicates that the light bands have significantly higher mean brightness than the dark bands. The p-value (3.26×10^{-22}) is extremely low, again confirming a highly significant difference between the two groups.

We additionally investigated the effect of illumination angle on the apparent grain size distribution in granular sandstones (see Supplementary Figure S3), using sandstone samples with different grain size ranges: A – >0.5 mm, B – 0.25–0.5 mm, and C – 0.1–0.25 mm. Grain size distributions were measured manually in ImageJ using the grid-intersection method, following Paola and Mohrig (1996) and Garefalakis et al. (2023). The analysed image size was 2.22 × 2.12 cm (566 × 540 pixels), and the area per point (grid cell) was 0.06 cm^2. To minimize bias, we measured the diameter of the grain closest to each grid intersection.

Our analysis showed no statistically significant differences in measured grain sizes under different lighting conditions, indicating that particle size estimates are largely robust to changes in illumination. However, diffused light improves the visual clarity of grain boundaries—especially for smaller grains—and makes grain shapes easier to discern. This improvement in visibility does not alter the quantitative results, but it facilitates manual measurements and highlights features such as lamination and compositional banding, which are marked by colour and intensity differences. Therefore, while lighting does not influence the grain size distribution itself, it does affect how easily key textural and compositional features—defined by colour and lustre—can be observed and interpreted (see Figure 8). This approach should also be applied and cross-validated using the CLUPI EM + model after colour correction is performed (see Section 2.3).

5 Discussion

5.1 Influence of illumination conditions on the recognition and differentiation of rock textures and morphological features

5.1.1 Identification of phenocrysts in igneous rocks

The analysis in Figure 8 shows the direct impact and importance of selecting preferred lighting conditions for distinguishing specific rock textures. For identifying phenocrysts in the igneous rock sample (Sample A), the high 70° midday solar angle is preferred. Although both lighting conditions (midday and evening/morning) are statistically significant ($p < 0.05$), the p-value is significantly smaller for midday conditions (9.06×10^{-9}) compared to evening/morning conditions (0.0113).

Examining the standard deviation (StdDev) values (Supplementary Table S1) reveals that under midday conditions, the phenocrysts group exhibited significantly higher contrast relative to the matrix, whereas in evening/morning conditions, the contrast between phenocrysts and matrix was much lower. Additionally, the difference in brightness was more pronounced under midday conditions, as indicated by the lower p-value, which signifies a stronger statistical difference.

This result can be attributed to the fact that certain phenocrysts and areas of the matrix in evening/morning light are significantly darker (e.g., phenocryst 1, with a mean brightness of 90 in midday light and 37 in evening/morning light), which are masked by shadows created by the low-angle light. This reduced contrast makes them more difficult to identify under evening/morning conditions. Conversely, some phenocrysts, such as phenocryst 6, appear overexposed in evening/morning light, with a mean brightness of 105 compared to 84 in midday conditions. These findings demonstrate that the p-values are lower for midday light, favouring these lighting conditions for distinguishing phenocrysts from the matrix more effectively.

In Sample B, the high 70° midday solar angle is also preferred for identifying white and black phenocrysts. The p-value is small (below 0.05) for both lighting conditions. However, the t-statistic for standard deviation (0.78; see Supplementary Table S1) indicates minimal contrast difference between white and black phenocrysts under evening/morning light. Under evening/morning light, some phenocrysts are obscured by shadows. For example, white phenocryst 4 had a mean brightness of 178 under midday light but only 80 under evening/morning light, making it more challenging to distinguish from black phenocrysts. Therefore, midday conditions, with reduced shadowing and enhanced contrast on the rock surface, are more effective for identifying phenocrysts.

5.1.2 Identification of laminations in sedimentary rocks

To identify fine laminations (0.02 mm in width) within the mudstone sample (Sample C), low-angle 25° illumination is demonstrated to be more effective. Under high-angle midday lighting, these laminations are not discernible to the naked eye due to their minimal size and low contrast. Quantitative analysis reveals that the mean brightness of the dark bands (strata) is approximately 111, while the mean brightness of the light bands (strata) is ~113, with a p-value of 0.5267 ($p > 0.05$). This indicates that the difference in mean brightness between the dark and light strata is not statistically significant, thus hindering the identification of laminations under these conditions.

In contrast, under low-angle 25° illumination, the mean brightness of the dark strata decreases significantly from ~111 to ~50, while the mean brightness of the light strata increases to ~128. This results in a substantial enhancement of contrast between the strata. The negative t-statistic (−14.06) confirms that the light bands exhibit significantly higher mean brightness compared to the dark bands, with an exceptionally low p-value (1.55×10^{-20}), indicating a highly significant difference between the two groups.

These findings underscore the critical role of low-angle illumination in enhancing the visibility of fine laminations, which are otherwise indiscernible under high-angle lighting. This approach is particularly valuable for the identification of laminated rock samples, which are considered promising targets due to their high potential for preserving biomarkers.

For larger laminations, such as those in the Pilbara stromatolites (0.5 mm width, Sample D), both high-angle 70° midday and low-angle 25° evening/morning illumination conditions are effective for their identification. In both cases, the contrast between dark bands (strata) and light bands remains high. Under midday lighting, the mean brightness of the dark bands is 56, and for the light bands, it is 141. Under low-angle lighting, the mean brightness of the dark bands increases to 75, and the light bands remain at 142, maintaining a strong contrast. The p-value for both lighting conditions is below 0.05, indicating statistical significance in the differentiation of dark and light strata.

Several factors contribute to the effective identification of laminations in this sample. Firstly, the laminations are wider compared to those in the mudstone sample (Sample C), making them more easily discernible. Secondly, the topography of the stromatolite sample is uneven, unlike the smoother topography of the mudstone, which generates additional shadows and enhances contrast, even under high-angle midday lighting. Lastly, different illumination conditions emphasise different types of information. Under high-angle 70° lighting, the colour differences between the darker and lighter strata, which are likely related to compositional variations, are more pronounced due to the absence of strong shadows. Conversely, low-angle lighting produces more pronounced shadows, masking some of the colour intensity differences between dark and light strata, but it highlights the morphological features of the laminations, such as deeper cracks and surface relief.

5.1.3 Effect of variable lighting on CLUPI's operation during the ExoMars mission

As CLUPI is an RGB camera and cannot perform mineralogical analyses, this example highlights its potential to distinguish between pixel intensity variations (e.g., dark and light bands) under midday lighting, which could subsequently be complemented with other instruments for compositional or mineralogical studies. Furthermore, our findings on the impact of varying illumination angles may inspire future advancements in filters and image post-processing strategies to enhance the recognition of features of interest in images captured under suboptimal lighting conditions. For instance, to detect sedimentary structures and potential morphological biosignatures, applying a filter that enhances contrast could improve the visibility of fine laminations. Conversely, reducing contrast in images might reveal hidden small-scale features, such as the shapes and sizes of phenocrysts and pebbles, enabling a more detailed evaluation of the samples.

Additionally, the ability to simulate high-angle (70°), low-angle (25°), and diffused lighting conditions can be achieved artificially during CLUPI operations. Since CLUPI is installed on a movable drill box (Josset et al., 2017), it is possible to manipulate lighting by altering the imaging angle. For example, an artificial shadow can be created by positioning the drill box to capture an image from a low angle, while minimizing shadows can be achieved by imaging directly from above. Diffused lighting could be simulated by completely covering the area above the sample with the drill box, preventing direct light from reaching the sample. These strategies provide greater flexibility in daily operations, allowing the science team to quickly adjust commands to optimise image acquisition under varying conditions.

However, it is important to note that sandstorms and dusk/dawn conditions significantly alter the spectral environment on Mars, even within the RGB domain that CLUPI can observe and resolve. During sandstorms, Mie scattering caused by suspended dust particles diffuses sunlight, reducing direct light, softening shadows, (e.g., Egan and Foreman, 1971) and shifting the colour balance towards the red spectrum, while reducing the intensity of blue and green channels. This results in muted colours, decreased contrast, and enhanced visibility of faint colour gradients or mineralogical variations within the rock matrix, though small-scale textures and cracks may become less discernible. Similarly, at dusk or dawn, the low solar angle increases the path length of sunlight through the atmosphere, enhancing Rayleigh scattering of shorter wavelengths, further shifting the spectral balance to red/orange hues. These conditions produce elongated shadows, which enhance contrast and highlight topographic features such as laminations or cracks, particularly in sedimentary rocks. Understanding these effects allows CLUPI to adapt its imaging strategies, using diffused light during sandstorms or low-angle shadows at dusk/dawn to enhance specific features, thereby maximising the scientific return under suboptimal illumination conditions.

5.2 Strategic planning for CLUPI at Oxia Planum

Based on the results from our CLUPI simulations on analogue rocks, we illustrate how identifying preferred light conditions for acquiring close-up images will be helpful during the strategic planning of the ExoMars mission. The results from the experimental simulations show that variable lighting conditions, especially the orientation of the illumination axis and the ratio between direct and diffused light, have a direct implication on distinguishing rock textures and structures. The information provided here will be helpful for the ExoMars science team in planning exploration strategies within Oxia Planum and aligning with the strategic science plan (Sefton-Nash et al., 2021; Sefton-Nash and Vago, 2024). It may also be useful for ongoing missions' science strategies, such as those for Curiosity and Perseverance (e.g., Grotzinger et al., 2012; Maki et al., 2020; Vasavada, 2022; Milkovich et al., 2022).

The preferred lighting conditions for identifying critical rock features can be effectively demonstrated through the development of exploration cascade decision trees for CLUPI. It is important to note that close-up visual information will likely be insufficient for unambiguously demonstrating the existence of past microbial life. Therefore, CLUPI images must be viewed as part of a holistic exploration cascade, together with other ExoMars analytical instruments determine the presence of biomarkers (Lopez-Reyes et al., 2020; Mitrofanov et al., 2017; Rull et al., 2017). Below, we present two such decision-making flowcharts for CLUPI, designed to aid in the exploration of two distinct areas within Oxia Planum (Figure 9).

The first target (Figure 10) was selected based on previous detections from remote sensing data at Oxia Planum, which revealed the possible presence of phyllosilicates, deltaic, and fluvial deposits—considered high-priority samples by the ExoMars Science Team. This target focuses on imaging and characterizing Layered Noachian Clays (lNc), Fluvial (Fd), and Deltaic (Dt) Deposits, which are critical for understanding the region's geological history and habitability potential.

The second target (Figure 11) while not identified by remote sensing, could include samples that would make compelling astrobiological targets if discovered during the mission. These could consist of hydrothermally altered rocks, evaporites, carbonates, and various sedimentary structures, potentially including morphological biosignatures. Such findings would significantly enhance the mission's scientific value, providing new insights into past environmental conditions and potential biosignature preservation.

5.2.1 Exploration strategy for detection of layered Noachian Clays (lNc) or fluvial (Fd) and deltaic (Dt) deposits

Target 1 (Figure 9) can host a large variety of rocks comprising both igneous and sedimentary rocks. The potential samples to be encountered are A- basalts within the Adru geological unit, B- laminated mudstone within the Dt, C - conglomerate and sandstones within Fd/Dt, and possibly stromatolite or any MISS, which could be associated with microbial activity (Noffke, 2009) and encountered anywhere in that region. As the primary scientific priority of ExoMars is to search for evidence of past life in Oxia Planum, the highest importance is given to detecting the Layered Noachian Clays (lNc) which can host and preserve the biosignatures with a secondary objective of detecting Fluvial (Fd) and Deltaic Deposits (Dt) to understand the past water activity in that region.

The first step to achieve this goal is to identify potential target rocks using PanCam, which provides a wide-field overview and multispectral imaging to determine the general composition and context of the area (Coates et al., 2017). PanCam can help distinguish between sedimentary and igneous rocks by analysing broad geological features and detecting spectral signatures indicative of specific rock types. Once a promising target is identified, ENFYS (which replaces ISEM-Infrared Spectrometer for ExoMars (Korablev et al., 2017) will be used for a more detailed mineralogical analysis. By measuring reflected infrared light, ENFYS can confirm the rock's composition and identify key minerals, further narrowing down whether the target is sedimentary or igneous.

Following PanCam and ENFYS observations, CLUPI is employed for close-up imaging to capture high-resolution details of the rock textures and structures (Josset et al., 2017). For igneous rocks, images are acquired using CLUPI under 70° daylight conditions, as this lighting angle is preferred for revealing textures such as vesicles or phenocrysts (Figure 10A). These features would be masked by shadows if observed under the 25° morning/evening light. For sedimentary rocks, the 25° morning/evening light is preferred, as it enhances contrast between fine-grained and coarse-grained textures, enabling detailed observation of sedimentary structures.

Once the sedimentary targets are identified, the further decision will be based on whether it is possible to see laminated, fine-grained rocks or granular, coarse-grained rocks (Figure 10B). Here, the exploration priority is given towards fine-grained sedimentary rocks as they could be related to Noachian clays, and they also have the highest likelihood of preserving biosignatures. The second series of image acquisition can take place in the morning or evening with a lower angle of 25° to further search for small-scale features that could be associated with aqueous or microbial activity, e.g., laminations in the Noachian clays (lNc) or in rare cases stromatolite laminae. This lower lighting condition of 25° is the best amongst the investigated options to create the contrast on the rock surface and therefore highlight these features (Figures 3D,E).

Once the laminations within the rock are studied, the third step would be to conduct the final, close-up observations of the material within the laminations or rock matrix where often Fe-Mg phyllosilicates are present (Figure 10C). Here it is worth mentioning that these clay minerals can be associated with both sedimentary rocks, such as mudstone which make a good drilling target as these rocks have a high likelihood of preserving biosignatures, but also within the weathered igneous rocks, such as altered phonolites, which are not the preferred candidates for biosignature preservation. To make such close-up observations, the diffused light of the lowest contrast should be applied as it creates the least contrast on the rock allowing investigation of colour differences within the laminations which could be related to the secondary minerals, including phyllosilicates (Figures 4B–F). These images can be captured under diffused light conditions, which provide preferred lighting for identifying small-scale features. Alternatively, when diffused light conditions are not available during the operational day, shadows cast by the rover or surrounding topography can be

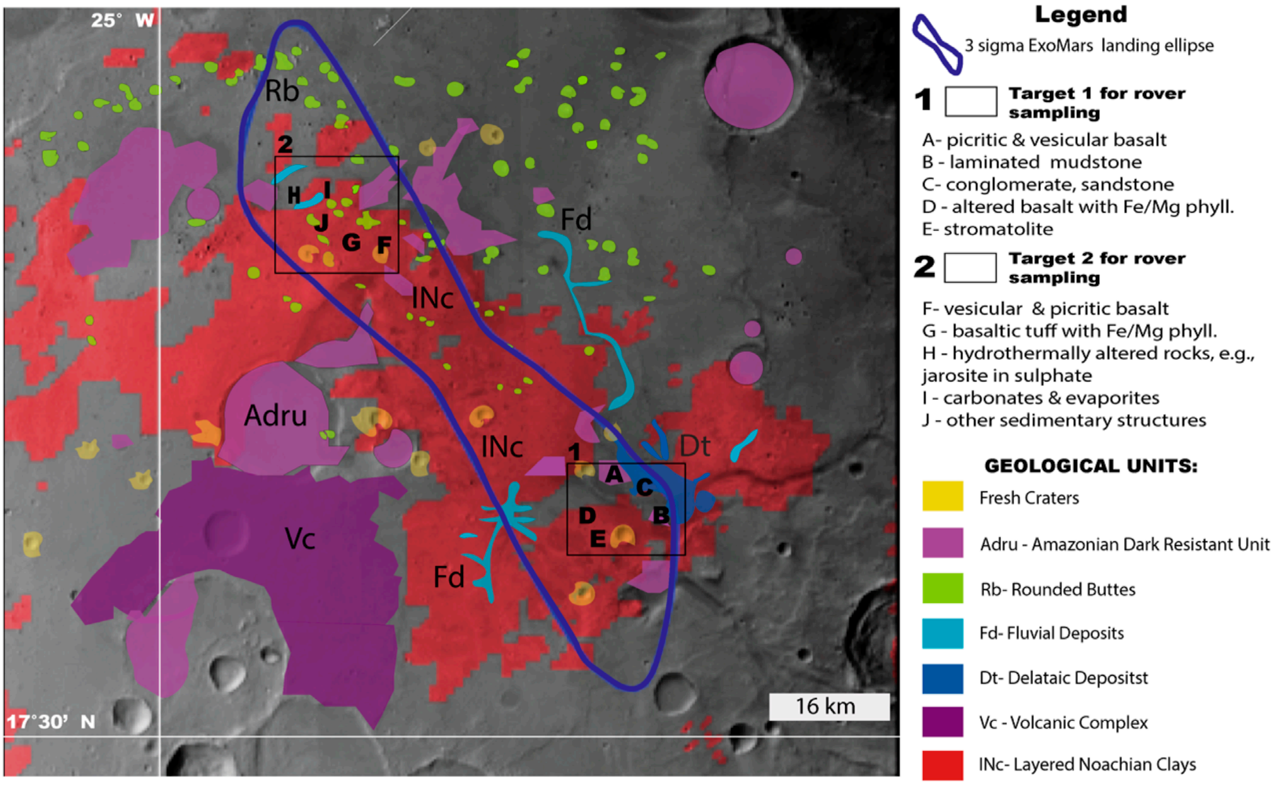

FIGURE 9
Geology of Oxia Planum with potential two exploration targets. The map was modified after (Quantin-Nataf et al., 2021).

used to minimize direct sunlight on the rock surface, producing diffused lighting conditions and allowing for the identification of small minerals within the laminations. For the clastic sedimentary rocks that could be found at Fluvial (Fd) and Deltaic (Dt) deposits, and can also be an interesting target for the ExoMars science team, it is advisable to use directly the diffused light (Figure 10D) for the final close-up investigation which is the most preferred (Figures 4A,B) as it creates the least shadow and contrast, allowing identification of pebbles, their size and orientation which can give a clue about the past Oxia's fluvial activity.

At the final stage, CLUPI will identify regions of interest in the selected samples for further complementary analyses with the rover's suite of analytical instruments, including Ma_MISS, MicroOmega, MOMA, Raman, and WISDOM (Korablev et al., 2017; Bibring et al., 2017; Goesmann et al., 2017; Rull et al., 2017; Ciarletti et al., 2017). These instruments will provide a comprehensive understanding of the sample's mineralogy, geochemistry, and potential biogenicity, offering insights into its habitability and past environmental conditions.

5.2.2 Exploration strategy for detection of hydrothermal alteration products, evaporites, carbonates, or other morphological features

Target 2 (Figure 9) is located within the INc unit with a high likelihood of finding Fe-Mg phyllosilicates, which could be additionally modified by aqueous processes due to the presence of fluvial deposits (Fd) and it also contains the Rounded Buttes (Rb) unit. This area is good to study an additional secondary science question of ExoMars, such as if there is evidence of past hydrothermal activity, active hydrothermal springs at Oxia during the Noachian period, or even the existence of a past ocean in that region. The potential samples to be encountered in this region are F - basalts within the Adru and Fresh crater geological unit, G - Fe/Mg phyllosilicates, H - hydrothermally altered rocks, e.g., jarosite in sulphate, and possibly I - carbonates and evaporites as well as J - other morphological features which could be formed by biotic processes. Here, the highest priority would be to detect potential carbonates and evaporites, morphological features and hydrothermally altered rocks (Figure 11). For that the three-stage exploration cascade was developed for each of these rocks.

As for the case of detecting Noachian Clays (INc), the first step would involve using PanCam (Coates et al., 2017) to provide a wide-field overview and multispectral imaging to identify areas of interest and distinguish between sedimentary and igneous rocks. PanCam would offer preliminary compositional data and guide the selection of potential targets for closer examination. Following PanCam, ENFYS would be deployed to perform shortwave infrared spectroscopy, identifying key minerals and confirming the nature of the rocks. Once PanCam and ENFYS observations indicate a promising target, the next step would involve acquiring images with CLUPI in the outcrop observation mode under daylight conditions with a solar angle of 70° to differentiate between sedimentary and igneous rocks (Figure 11A). If the sedimentary rocks show any signs of structures such as spherules, cracks, polygons, laminae, the

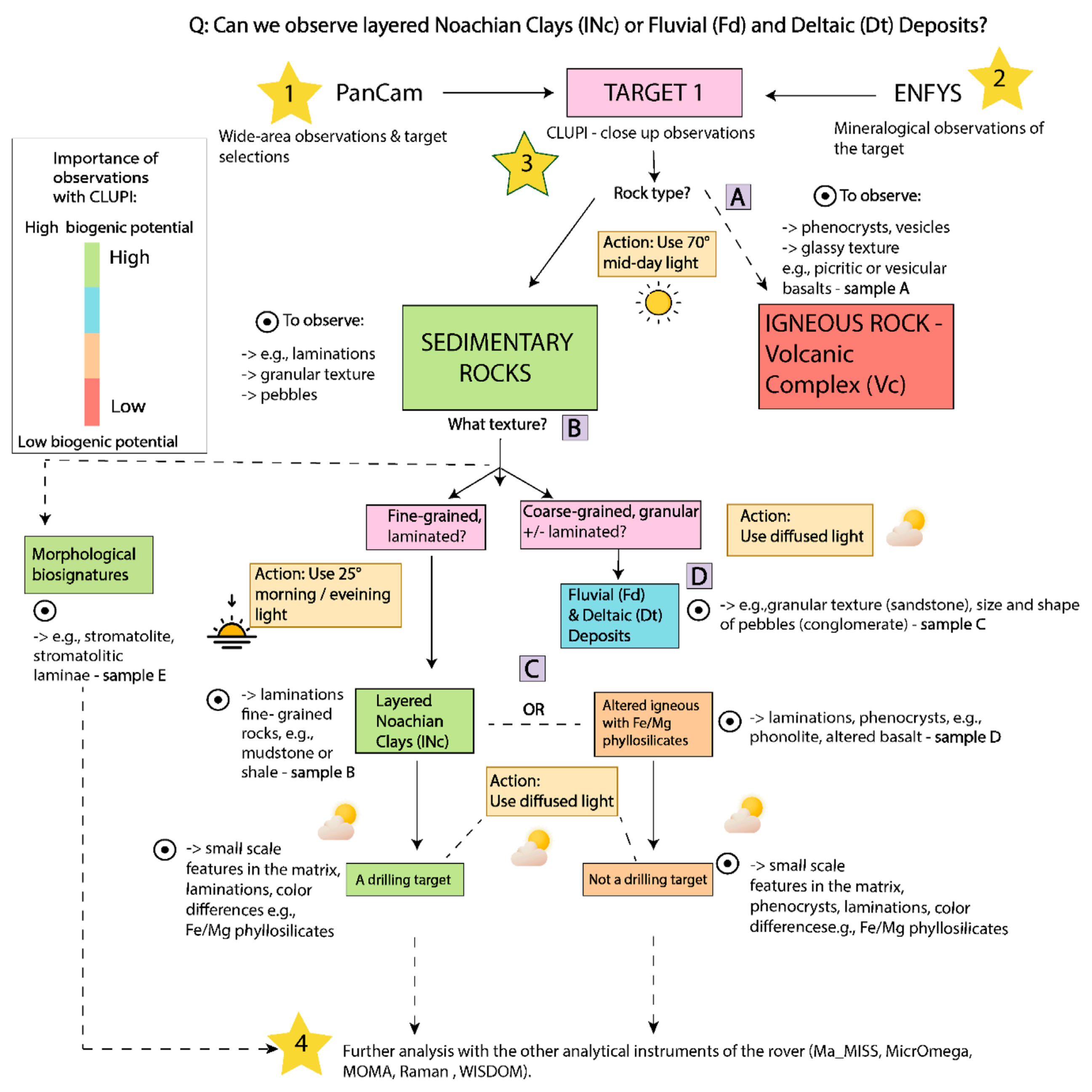

FIGURE 10
Exploration strategy and decision tree for CLUPI to detect Noachian Clays (Inc) or Fluvial (Fd) and Deltaic Deposits (Dt). Starting from 1 - wide-area observation and target selection by PanCam, 2- mineralogical observations of the target with ENFYS, and 3- close up-observations with CLUPI: **(A)** preferred conditions to capture the rock type; **(B)** preferred conditions to recognize rock texture; C- preferred conditions to recognize the small-scale features; **(D)** preferred conditions to recognize Fluvial (Fd) and Deltaic (Dt) deposits. The exploration ends with 4- further analysis with other analytical instruments of ExoMars rover.

low angle of morning/evening 25° light conditions can be used to look at these features closer with the contrasting light to deduce whether they are associated with the biogenic (MISS) or abiogenic (aeolian, weathering, etc.) features (Figure 11B). If the rocks are fine-grained and do not show the structures, applying the diffused light (Figure 11C) could be the most efficient to make follow-up, close-up observations on details such as carbonate rock matrix and gypsum (Figures 6C,D). The follow-up investigations with diffused light could take place to further search for Fe-Mg phyllosilicates within the identified rock textures or search for colour differences (e.g., scouting for yellow minerals, Figures 6A,B) could also take place in this region to possibly find the jarosite or any other precipitated mineral within the rock matrix that could have been deposited by hydrothermal alteration.

Gypsum, carbonates or hydrothermally altered sedimentary rocks are a drilling target because of their potential to preserve

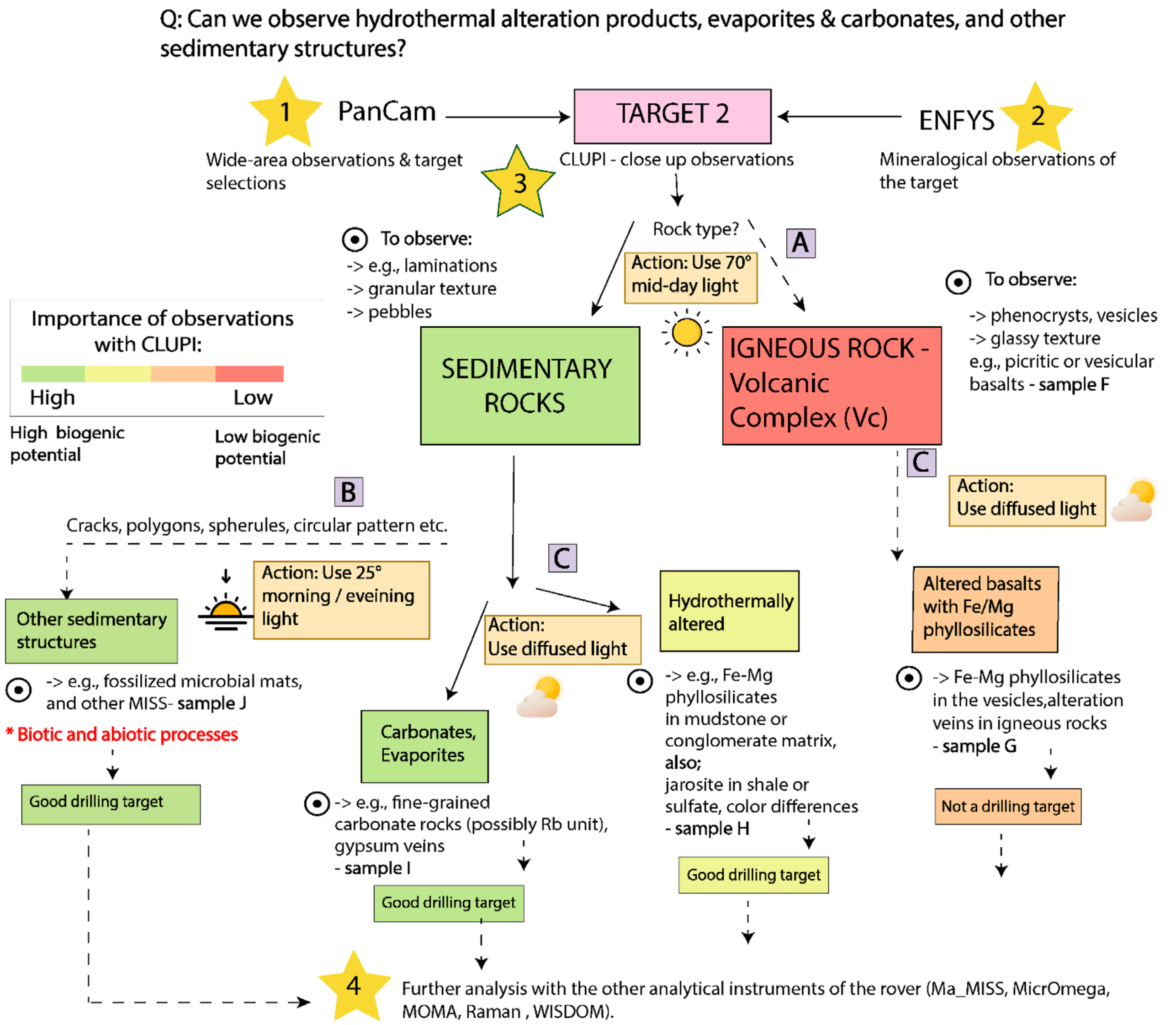

FIGURE 11
Exploration strategy and decision tree for CLUPI to detect hydrothermal alteration products, evaporites, carbonates and other sedimentary structures). Starting from 1 - wide-area observation and target selection by PanCam, 2- mineralogical observations of the target with ENFYS, and 3- close up-observations with CLUPI: **(A)** preferred conditions to capture the rock type; **(B)** preferred conditions to identify rock texture; C- preferred conditions to recognize the small-scale features. The exploration ends with 4- further analysis with other analytical instruments of ExoMars rover.

biosignatures. If found at Oxia, they would make a suitable drilling target for potential biosignature detection and answering questions regarding the hydrothermal activity at Oxia in Noachian. Features, such as cracks, spherules or polygons could also be an interesting target due to the possibility of detecting MISS. Moreover, third-priority samples could include hydrothermally altered igneous rocks with Fe-Mg phyllosilicates in the veins (Krzesińska et al., 2021), which could be studied by CLUPI under diffused lighting conditions to highlight the presence of small minerals, such as phyllosilicates within the veins and laminations.

Finally, the regions of interest identified by CLUPI would undergo complementary analyses using the rover's suite of analytical instruments (see previous section).

6 Conclusion

The findings of our study have led to the creation of an image catalogue featuring rocks expected to be found in Oxia Planum. Our results highlight the significant impact that varying illumination conditions—specifically, the orientation of the illumination axis, the angle of incident light (e.g., high angle 70° midday vs low angle 25° morning/evening), and the ratio between direct and diffused light—on the ability to distinguish rock textures and sedimentary structures in close-up imagery. We found that a high angle (70°) is preferred for recognising phenocrysts in igneous rocks and differences in colour intensities or brightness, a low angle (25°) is preferred for identifying laminations in sedimentary rocks, and diffused light is most effective for small-scale observations within the rock matrix. We have demonstrated that by strategically capturing images at different times of the day under specific lighting conditions, it becomes possible to increase the likelihood of detecting diverse rock textures and relevant structures. These findings have the potential to increase the scientific return of the collected data, contributing to a better understanding of Oxia Planum and supporting scientists in decision-making during ExoMars rover mission.

Data availability statement

The original contributions presented in the study are included in the article/Supplementary Material, further inquiries can be directed to the corresponding author.

Author contributions

GL: Conceptualization, Data curation, Formal Analysis, Investigation, Methodology, Visualization, Writing – original draft, Writing – review and editing. TB: Conceptualization, Supervision, Validation, Writing – review and editing. LF: Validation, Writing – review and editing. AB: Writing – review and editing. BH: Resources, Writing – review and editing. J-LJ: Funding acquisition, Resources, Writing – review and editing. NK: Conceptualization, Funding acquisition, Resources, Supervision, Writing – review and editing.

Funding

The author(s) declare that financial support was received for the research and/or publication of this article. This work is supported by the Swiss National Science Foundation (grant 200021_197293).

Acknowledgments

We express our gratitude to Agata Krzesinska and Stephanie Werner from University of Oslo from PTAL (The Planetary Terrestrial Analogues Library) and Leander Franz from the University of Basel for providing analogue rock samples for this study. Additionally, we thank Martin Koziol of the Maarmuseum in Manderscheid and Rech Kies GmbH in Oberkail for assisting in organizing the fieldwork to the Eifel Volcanic Province in Germany to collect igneous and sedimentary samples. Special appreciation goes to Brigitte NK for her technical advice on image acquisition with the Canon camera, and to Josephine Pausch and Ciara Schober for their assistance with image acquisition at the Marslabor. This work is supported by the Swiss National Science Foundation (grant 20021_197293).

Conflict of interest

The authors declare that the research was conducted in the absence of any commercial or financial relationships that could be construed as a potential conflict of interest.

Generative AI statement

The author(s) declare that no Generative AI was used in the creation of this manuscript.

Publisher's note

Supplementary material

The Supplementary Material for this article can be found online at: https://www.frontiersin.org/articles/10.3389/fspas.2025.1530408/full#supplementary-material

References

Achilles, C. N., Rampe, E. B., Downs, R. T., Bristow, T. F., Ming, D. W., Morris, R. V., et al. (2020). Evidence for multiple diagenetic episodes in ancient fluvial-lacustrine sedimentary rocks in Gale crater, Mars. *J. Geophys. Res. Planets* 125 (8), e2019JE006295. doi:10.1029/2019JE006295

Allwood, A., Clark, B., Flannery, D., Hurowitz, J., Wade, L., Elam, T., et al. (2015). "Texture-specific elemental analysis of rocks and soils with PIXL: the planetary instrument for X-ray lithochemistry on mars 2020," in *2015 IEEE aerospace conference* (IEEE), 1–13. doi:10.1109/AERO.2015.7119099

Allwood, A. C., Burch, I. W., Rouchy, J. M., and Coleman, M. (2013). Morphological biosignatures in gypsum: diverse formation processes of Messinian (~ 6.0 Ma) gypsum stromatolites. *Astrobiology* 13 (9), 870–886. doi:10.1089/ast.2013.1021

Allwood, A. C., Walter, M. R., Burch, I. W., and Kamber, B. S. (2007). 3.43 billion-year-old stromatolite reef from the Pilbara Craton of Western Australia: ecosystem-scale insights to early life on Earth. *Precambrian Res.* 158 (3-4), 198–227. doi:10.1016/j.precamres.2007.04.013

Appelbaum, J., and Flood, D. J. (1990). Solar radiation on mars. *Sol. Energy* 45 (6), 353–363. doi:10.1016/0038-092X(90)90156-7

Appelbaum, J., Landis, G. A., and Sherman, I. (1993). Solar radiation on Mars—update 1991. *Sol. Energy* 50 (1), 35–51. doi:10.1016/0038-092X(93)90006-A

April, R. H., and Keller, D. M. (1992). Saponite and vermiculite in amygdales of the Granby basaltic tuff, Connecticut Valley. *Clays Clay Minerals* 40 (1), 22–31. doi:10.1346/CCMN.1992.0400104

Awramik, S. M. (1992). "The history and significance of stromatolites," in *Early organic evolution: implications for mineral and energy resources* (Berlin, Heidelberg: Springer Berlin Heidelberg), 435–449. doi:10.1007/978-3-642-76884-2_34

Banham, S. G., Gupta, S., Rubin, D. M., Bedford, C. C., Edgar, L. A., Bryk, A. B., et al. (2022). Evidence for fluctuating wind in shaping an ancient Martian dune field: the Stimson formation at the Greenheugh pediment, Gale crater. *J. Geophys. Res. Planets* 127 (9), e2021JE007023. doi:10.1029/2021JE007023

Banham, S. G., Gupta, S., Rubin, D. M., Watkins, J. A., Sumner, D. Y., Edgett, K. S., et al. (2018). Ancient Martian aeolian processes and palaeomorphology reconstructed from the Stimson formation on the lower slope of Aeolis Mons, Gale crater, Mars. *Sedimentology* 65 (4), 993–1042. doi:10.1111/sed.12469

Bennett, K. A., Fox, V. K., Bryk, A., Dietrich, W., Fedo, C., Edgar, L., et al. (2023). The Curiosity rover's exploration of Glen Torridon, Gale crater, Mars: an overview of the campaign and scientific results. *J. Geophys. Res. Planets* 128 (1), e2022JE007185. doi:10.1029/2022JE007185

Bibring, J. P., Hamm, V., Pilorget, C., Vago, J. L., the MicrOmega Team, (2017). The micrOmega investigation onboard ExoMars. *Astrobiology* 17 (6-7), 621–626. doi:10.1089/ast.2016.1642

Bontognali, T., Blattmann, F., Al Disi, Z., Al Saad Al Kuwari, H., DiLoreto, Z., Dittrich, M., et al. (2020). "The sabkhas of Qatar: modern analogues for studying early life on Earth and on Mars," in *EGU general assembly conference abstracts*. doi:10.5194/egusphere-egu2020-21629

Bontognali, T. R., Meister, Y., Kuhn, B., Josset, J. L., Hofmann, B. A., and Kuhn, N. (2021). Identifying optimal working conditions for close-up imagining during the ExoMars rover mission. *Planet. space Sci.* 208, 105355. doi:10.1016/j.pss.2021.105355

Bontognali, T. R., Sessions, A. L., Allwood, A. C., Fischer, W. W., Grotzinger, J. P., Summons, R. E., et al. (2012). Sulfur isotopes of organic matter preserved in 3.45-billion-year-old stromatolites reveal microbial metabolism. *Proc. Natl. Acad. Sci.* 109 (38), 15146–15151. doi:10.1073/pnas.1207491109

Bosak, T., Moore, K. R., Gong, J., and Grotzinger, J. P. (2021). Searching for biosignatures in sedimentary rocks from early Earth and Mars. *Nat. Rev. Earth and Environ.* 2 (7), 490–506. doi:10.1038/s43017-021-00169-5

Bost, N., Westall, F., Ramboz, C., Foucher, F., Pullan, D., Meunier, A., et al. (2013). Missions to mars: characterisation of mars analogue rocks for the international space analogue rockstore (ISAR). *Planet. Space Sci.* 82, 113–127. doi:10.1016/j.pss.2013.04.006

Bouquety, A., Fayon, L., Koschny, D., Narbey, R., Bontognali, T. R., Jorda, L., et al. (2024). Preparation of the ExoMars Mission: feasibility study and preliminary methods for generating stereoscopic data with the CLose-UP Imager CLUPI. *Adv. Space Res.* 75, 1528–1541. doi:10.1016/j.asr.2024.09.006

Braunger, S., Marks, M. A. W., Walter, B. F., Neubauer, R., Reich, R., Wenzel, T., et al. (2018). The petrology of the Kaiserstuhl Volcanic Complex, SW Germany: the importance of metasomatized and oxidized lithospheric mantle for carbonatite generation. *J. Petrol.* 59 (9), 1731–1762. doi:10.1093/petrology/egy078

Brossier, J., Altieri, F., De Sanctis, M. C., Frigeri, A., Ferrari, M., De Angelis, S., et al. (2022). Constraining the spectral behavior of the clay-bearing outcrops in Oxia Planum, the landing site for ExoMars "Rosalind Franklin" rover. *Icarus* 386, 115114. doi:10.1016/j.icarus.2022.115114

Christensen, P. R., McSween Jr, H. Y., Bandfield, J. L., Ruff, S. W., Rogers, A. D., Hamilton, V. E., et al. (2005). Evidence for magmatic evolution and diversity on Mars from infrared observations. *Nature* 436 (7050), 504–509. doi:10.1038/nature03639

Ciarletti, V., Clifford, S., Plettemeier, D., Le Gall, A., Hervé, Y., Dorizon, S., et al. (2017). The WISDOM radar: unveiling the subsurface beneath the ExoMars Rover and identifying the best locations for drilling. *Astrobiology* 17 (6-7), 565–584. doi:10.1089/ast.2016.1532

Clave, E., Benzerara, K., Meslin, P. Y., Forni, O., Royer, C., Mandon, L., et al. (2023). Carbonate detection with SuperCam in igneous rocks on the floor of Jezero crater, mars. *J. Geophys. Res. Planets* 128 (6), e2022JE007463. doi:10.1029/2022JE007463

Coates, A. J., Jaumann, R., Griffiths, A. D., Leff, C. E., Schmitz, N., Josset, J. L., et al. (2017). The PanCam instrument for the ExoMars rover. *Astrobiology* 17 (6-7), 511–541. doi:10.1089/ast.2016.1548

Cockell, C. S., McMahon, S., Lim, D. S., Rummel, J., Stevens, A., Hughes, S. S., et al. (2019). Sample collection and return from Mars: optimising sample collection based on the microbial ecology of terrestrial volcanic environments. *Space Sci. Rev.* 215, 44–25. doi:10.1007/s11214-019-0609-7

Craw, D., Smith, D. W., and Youngson, J. H. (1995). Formation of authigenic Fe2+-bearing smectite-vermiculite during terrestrial diagenesis, southern New Zealand. *N. Z. J. Geol. Geophys.* 38 (2), 151–158. doi:10.1080/00288306.1995.9514647

Crumpler, L. S., McCoy, T., and Schmidt, M. (2007). "Spirit: observations of very vesicular basalts in the columbia hills, mars and significance for primary lava textures, volatiles, and paleoenvironment," in *38th annual lunar and planetary science conference*, 2298.

Davies, N. S., Liu, A. G., Gibling, M. R., and Miller, R. F. (2016). Resolving MISS conceptions and misconceptions: a geological approach to sedimentary surface textures generated by microbial and abiotic processes. *Earth-Science Rev.* 154, 210–246. doi:10.1016/j.earscirev.2016.01.005

Davis, J. M., Balme, M. R., Fawdon, P., Grindrod, P. M., Favaro, E. A., Banham, S. G., et al. (2023). Ancient alluvial plains at Oxia Planum, mars. *Earth Planet. Sci. Lett.* 601, 117904. doi:10.1016/j.epsl.2022.117904

Day-Stirrat, R. J., Aplin, A. C., Środoń, J., and Van der Pluijm, B. A. (2008). Diagenetic reorientation of phyllosilicate minerals in Paleogene mudstones of the Podhale Basin, southern Poland. *Clays Clay Minerals* 56 (1), 100–111. doi:10.1346/CCMN.2008.0560109

De Sanctis, M. C., Altieri, F., Ammannito, E., Biondi, D., De Angelis, S., Meini, M., et al. (2017). Ma_MISS on ExoMars: mineralogical characterization of the martian subsurface. *Astrobiology* 17 (6-7), 612–620. doi:10.1089/ast.2016.1541

Dietrich, W. E., Palucis, M. C., Williams, R. M., Lewis, K. W., Rivera-Hernandez, F., and Sumner, D. Y. (2017). Fluvial gravels on mars: analysis and implications. *Gravel-Bed Rivers Process. Disasters*, 755–783. doi:10.1002/9781118971437.ch28

Diloreto, Z., Ahmad, M. S., Al Saad Al-Kuwari, H., Sadooni, F., Bontognali, T. R., and Dittrich, M. (2023). Raman spectroscopic and microbial study of biofilms hosted gypsum deposits in the hypersaline wetlands: astrobiological perspective. *Astrobiology* 23 (9), 991–1005. doi:10.1089/ast.2023.0003

Eberl, D. D. (2022). On the formation of Martian blueberries. *Am. Mineralogist* 107 (1), 153–155. doi:10.2138/am-2022-8167

Edgar, L. A., Gupta, S., Rubin, D. M., Lewis, K. W., Kocurek, G. A., Anderson, R. B., et al. (2018). Shaler: *in situ* analysis of a fluvial sedimentary deposit on Mars. *Sedimentology* 65 (1), 96–122. doi:10.1111/sed.12370

Egan, W. G., and Foreman, K. M. (1971). Mie scattering and the Martian atmosphere. *Symposium-International Astron. Union* 40, 156–165. doi:10.1017/S0074180900102712

Ehlmann, B. L., Mustard, J. F., Murchie, S. L., Poulet, F., Bishop, J. L., Brown, A. J., et al. (2008). Orbital identification of carbonate-bearing rocks on Mars. *Science* 322 (5909), 1828–1832. doi:10.1126/science.1164759

Eigenbrode, J. L., Summons, R. E., Steele, A., Freissinet, C., Millan, M., Navarro-González, R., et al. (2018). Organic matter preserved in 3-billion-year-old mudstones at Gale crater, Mars. *Science* 360 (6393), 1096–1101. doi:10.1126/science.aas9185

El Maarry, M. R., Markiewicz, W. J., Mellon, M. T., Goetz, W., Dohm, J. M., and Pack, A. (2010). Crater floor polygons: desiccation patterns of ancient lakes on Mars? *J. Geophys. Res. Planets* 115 (E10). doi:10.1029/2010JE003609

Elwood Madden, M. E., Bodnar, R. J., and Rimstidt, J. D. (2004). Jarosite as an indicator of water-limited chemical weathering on Mars. *Nature* 431 (7010), 821–823. doi:10.1038/nature02971

Fairén, A. G., Schulze-Makuch, D., Rodríguez, A. P., Fink, W., Davila, A. F., Uceda, E. R., et al. (2009). Evidence for Amazonian acidic liquid water on Mars—a reinterpretation of MER mission results. *Planet. Space Sci.* 57 (3), 276–287. doi:10.1016/j.pss.2008.11.008

Farrand, W. H., Glotch, T. D., Rice Jr, J. W., Hurowitz, J. A., and Swayze, G. A. (2009). Discovery of jarosite within the Mawrth Vallis region of Mars: implications for the geologic history of the region. *Icarus* 204 (2), 478–488. doi:10.1016/j.icarus.2009.07.014

Fawdon, P., Balme, M., Davis, J., Bridges, J., Gupta, S., and Quantin-Nataf, C. (2022). Rivers and lakes in Western Arabia Terra: the fluvial catchment of the ExoMars 2022 rover landing site. *J. Geophys. Res. Planets* 127 (2), e2021JE007045. doi:10.1029/2021JE007045

Foucher, F., Bost, N., Guimbretière, G., Courtois, A., Hickman-Lewis, K., Marceau, E., et al. (2022). Igneous rock powder identification using colour cameras: a powerful method for space exploration. *Icarus* 375, 114848. doi:10.1016/j.icarus.2021.114848

Garefalakis, P., do Prado, A. H., Mair, D., Douillet, G. A., Nyffenegger, F., and Schlunegger, F. (2023). Comparison of three grain size measuring methods applied to coarse-grained gravel deposits. *Sediment. Geol.* 446, 106340. doi:10.1016/j.sedgeo.2023.106340

Gill, K. K., Jagniecki, E. A., Benison, K. C., and Gibson, M. E. (2023). A Mars-analog sulfate mineral, mirabilite, preserves biosignatures. *Geology* 51 (9), 818–822. doi:10.1130/G51256.1

Goesmann, F., Brinckerhoff, W. B., Raulin, F., Goetz, W., Danell, R. M., Getty, S. A., et al. (2017). The Mars Organic Molecule Analyzer (MOMA) instrument: characterization of organic material in martian sediments. *Astrobiology* 17 (6-7), 655–685. doi:10.1089/ast.2016.1551

Grotzinger, J. P. (2013). Analysis of surface materials by the Curiosity Mars rover. *Science* 341 (6153), 1475. doi:10.1126/science.1244258

Grotzinger, J. P., Arvidson, R. E., Bell Iii, J. F., Calvin, W., Clark, B. C., Fike, D. A., et al. (2005). Stratigraphy and sedimentology of a dry to wet eolian depositional system, Burns formation, Meridiani Planum, Mars. *Earth Planet. Sci. Lett.* 240 (1), 11–72. doi:10.1016/j.epsl.2005.09.039

Grotzinger, J. P., Crisp, J., Vasavada, A. R., Anderson, R. C., Baker, C. J., Barry, R., et al. (2012). Mars Science Laboratory mission and science investigation. *Space Sci. Rev.* 170, 5–56. doi:10.1007/s11214-012-9892-2

Guerrero, M. C., and De Wit, R. (1992). Microbial mats in the inland saline lakes of Spain. *Limnetica* 8, 197–204. doi:10.23818/limn.08.19

Hamilton, V. E., and Christensen, P. R. (2005). Evidence for extensive, olivine-rich bedrock on Mars. *Geology* 33 (6), 433–436. doi:10.1130/G21258.1

Hauber, E., Tirsch, D., Adeli, S., Acktories, S., Steffens, S., and Nass, A. (2021). "Regional geologic mapping of the oxia planum landing site for the exomars 2022 mission," in 52nd Lunar and Planetary Science Conference, 15-19 March 2021. doi:10.5194/egusphere-egu21-12178

Hayes, A. G., Grotzinger, J. P., Edgar, L. A., Squyres, S. W., Watters, W. A., and Sohl-Dickstein, J. (2011). Reconstruction of eolian bed forms and paleocurrents from cross-bedded strata at Victoria Crater, Meridiani Planum, Mars. *J. Geophys. Res. Planets* 116 (E7), E00F21. doi:10.1029/2010JE003688

Hickman-Lewis, K., Foucher, F., Pelletier, S., Messori, F., and Westall, F. (2020). Geological appraisals of core samples using the ExoMars 2020 rover instrumentation. *Planet. Space Sci.* 180, 104743. doi:10.1016/j.pss.2019.104743

Homann, M. (2019). Earliest life on earth: evidence from the barberton greenstone belt, South Africa. *Earth-Science Rev.* 196, 102888. doi:10.1016/j.earscirev.2019.102888

Homann, M., Sansjofre, P., Van Zuilen, M., Heubeck, C., Gong, J., Killingsworth, B., et al. (2018). Microbial life and biogeochemical cycling on land 3,220 million years ago. *Nat. Geosci.* 11 (9), 665–671. doi:10.1038/s41561-018-0190-9

Joseph, R. A., and Armstrong, R. (2022). Mollusks on mars! Rock-boring marine life in jazero crater: a comparative quantitative morphological analysis. *J. Cosmol.* 32, 44–85. Available online at: https://www.researchgate.net/publication/361426747

Josset, J. L., Westall, F., Hofmann, B. A., Spray, J., Cockell, C., Kempe, S., et al. (2017). The Close-Up Imager onboard the ESA ExoMars Rover: objectives, description, operations, and science validation activities. *Astrobiology* 17 (6-7), 595–611. doi:10.1089/ast.2016.1546

Kminek, G., and Bada, J. L. (2006). The effect of ionizing radiation on the preservation of amino acids on Mars. *Earth Planet. Sci. Lett.* 245 (1-2), 1–5. doi:10.1016/j.epsl.2006.03.008

Korablev, O. I., Dobrolensky, Y., Evdokimova, N., Fedorova, A. A., Kuzmin, R. O., Mantsevich, S. N., et al. (2017). Infrared spectrometer for ExoMars: a mast-mounted instrument for the rover. *Astrobiology* 17 (6-7), 542–564. doi:10.1089/ast.2016.1543

Krzesińska, A. M., Bultel, B., Loizeau, D., Craw, D., April, R., Poulet, F., et al. (2021). Mineralogical and spectral (near-infrared) characterization of Fe-rich vermiculite-bearing terrestrial deposits and constraints for mineralogy of oxia planum, ExoMars 2022 landing site. *Astrobiology* 21 (8), 997–1016. doi:10.1089/ast.2020.2410

Liu, Y., Tice, M. M., Schmidt, M. E., Treiman, A. H., Kizovski, T. V., Hurowitz, J. A., et al. (2022). An olivine cumulate outcrop on the floor of Jezero crater, Mars. *Science* 377 (6614), 1513–1519. doi:10.1126/science.abo2756

Lopez-Reyes, G., Pilorget, C., Moral, A. G., Manrique, J. A., Sanz, A., Berrocal, A., et al. (2020). Raman Laser Spectrometer (RLS) calibration target design to allow onboard combined science between the RLS and MicrOmega instruments on the ExoMars rover. *J. Raman Spectrosc.* 51 (9), 1718–1730. doi:10.1002/jrs.5832

Maki, J. N., Gruel, D., McKinney, C., Ravine, M. A., Morales, M., Lee, D., et al. (2020). The Mars 2020 Engineering Cameras and microphone on the perseverance rover: a next-generation imaging system for Mars exploration. *Space Sci. Rev.* 216, 137–148. doi:10.1007/s11214-020-00765-9

Mandon, L., Parkes, A. B., Quantin-Nataf, C., Bridges, J. C., Carter, J., and Pan, L. (2019). "Spectral diversity and stratigraphy of the clay-bearing unit at the ExoMars 2020 landing site Oxia Planum," in *Ninth international conference on Mars*, 6173.

Mandon, L., Parkes Bowen, A., Quantin-Nataf, C., Bridges, J. C., Carter, J., Pan, L., et al. (2021). Morphological and spectral diversity of the clay-bearing unit at the ExoMars landing site Oxia Planum. *Astrobiology* 21 (4), 464–480. doi:10.1089/ast.2020.2292

Mangold, N., Gupta, S., Gasnault, O., Dromart, G., Tarnas, J. D., Sholes, S. F., et al. (2021). Perseverance rover reveals an ancient delta-lake system and flood deposits at Jezero crater, Mars. *Science* 374 (6568), 711–717. doi:10.1126/science.abl4051

Martínez-Frías, J., Lunar, R., Rodríguez-Losada, J. A., Delgado, A., and Rull, F. (2004). The volcanism-related multistage hydrothermal system of El Jaroso (SE Spain): implications for the exploration of Mars. *Earth, planets space* 56, v–viii. doi:10.1186/BF03352523

McIntosh, O., García-Florentino, C., Fornaro, T., Marabello, D., Alberini, A., Siljeström, S., et al. (2024). Undecanoic acid and L-phenylalanine in vermiculite: detection, characterization, and UV degradation studies for biosignature identification on mars. *Astrobiology* 24 (5), 518–537. doi:10.1089/ast.2023.0088

McNeil, J. D., Fawdon, P., Balme, M. R., and Coe, A. L. (2021). Morphology, morphometry and distribution of isolated landforms in southern Chryse Planitia, Mars. *J. Geophys. Res. Planets* 126 (5), e2020JE006775. doi:10.1029/2020JE006775

McSween, H. Y., Wyatt, M. B., Gellert, R., Bell III, J. F., Morris, R. V., Herkenhoff, K. E., et al. (2006). Characterization and petrologic interpretation of olivine-rich basalts at Gusev Crater, Mars. *J. Geophys. Res. Planets* 111 (E2). doi:10.1029/2005JE002477

Mège, D., Gurgurewicz, J., Massironi, M., Pozzobon, R., Tognon, G., Pajola, M., et al. (2023). Hydrothermal alteration of ultramafic rocks in ladon basin, mars—insights from CaSSIS, HiRISE, CRISM, and CTX. *J. Geophys. Res. Planets* 128 (1), e2022JE007223. doi:10.1029/2022JE007223

Meunier, A. (1995). "Hydrothermal alteration by veins," in *Origin and mineralogy of clays: clays and the environment* (Berlin, Heidelberg: Springer Berlin Heidelberg), 247–267. doi:10.1007/978-3-662-12648-6_6

Michalski, J. R., and Niles, P. B. (2010). Deep crustal carbonate rocks exposed by meteor impact on Mars. *Nat. Geosci.* 3 (11), 751–755. doi:10.1038/ngeo971

Milkovich, S. M., Stack, K. M., Sun, V. Z., Maxwell, K., Kronyak, R., Schnadt, S. L., et al. (2022). "Balancing predictive and reactive science planning for Mars 2020 perseverance," in *2022 IEEE aerospace conference (AERO)* (IEEE), 1–12. doi:10.1109/AERO53065.2022.9843572

Mitrofanov, I. G., Litvak, M. L., Nikiforov, S. Y., Jun, I., Bobrovnitsky, Y. I., Golovin, D. V., et al. (2017). The ADRON-RM instrument onboard the ExoMars Rover. *Astrobiology* 17 (6-7), 585–594. doi:10.1089/ast.2016.1566

Morris, R. V., Ruff, S. W., Gellert, R., Ming, D. W., Arvidson, R. E., Clark, B. C., et al. (2010). Identification of carbonate-rich outcrops on Mars by the Spirit rover. *Science* 329 (5990), 421–424. doi:10.1126/science.1189667

Mustard, J. F., Poulet, F., Gendrin, A., Bibring, J. P., Langevin, Y., Gondet, B., et al. (2005). Olivine and pyroxene diversity in the crust of Mars. *Science* 307 (5715), 1594–1597. doi:10.1126/science.1109098

Mustoe, G. E. (1982). The origin of honeycomb weathering. *Geol. Soc. Am. Bull.* 93 (2), 108–115. doi:10.1130/0016-7606(1982)93<108:TOOHW>2.0.CO;2

Mustoe, G. E. (2010). Biogenic origin of coastal honeycomb weathering. *Earth Surf. Process. Landforms* 35 (4), 424–434. doi:10.1002/esp.1931

Nachon, M., Clegg, S. M., Mangold, N., Schröder, S., Kah, L. C., Dromart, G., et al. (2014). Calcium sulfate veins characterized by ChemCam/Curiosity at Gale crater, Mars. *J. Geophys. Res. Planets* 119 (9), 1991–2016. doi:10.1002/2013JE004588

Noffke, N. (2009). The criteria for the biogeneicity of microbially induced sedimentary structures (MISS) in Archean and younger, sandy deposits. *Earth-Science Rev.* 96 (3), 173–180. doi:10.1016/j.earscirev.2008.08.002

Noffke, N. (2010). *Geobiology: microbial mats in sandy deposits from the Archean Era to today*. Springer Science and Business Media.

Noffke, N. (2021). Microbially induced sedimentary structures in clastic deposits: implication for the prospection for fossil life on Mars. *Astrobiology* 21 (7), 866–892. doi:10.1089/ast.2021.0011

Noffke, N., Gerdes, G., Klenke, T., and Krumbein, W. E. (2001). Microbially induced sedimentary structures: a new category within the classification of primary sedimentary structures. *J. Sediment. Res.* 71 (5), 649–656. doi:10.1306/2DC4095D-0E47-11D7-8643000102C1865D

Paola, C., and Mohrig, D. (1996). Palaeohydraulics revisited: palaeoslope estimation in coarse-grained braided rivers. *Basin Res.* 8 (3), 243–254. doi:10.1046/j.1365-2117.1996.00253.x

Peretyazhko, T. S., Sutter, B., Morris, R. V., Agresti, D. G., Le, L., and Ming, D. W. (2016). Fe/Mg smectite formation under acidic conditions on early Mars. *Geochimica Cosmochimica Acta* 173, 37–49. doi:10.1016/j.gca.2015.10.012

Playter, T., Konhauser, K., Owttrim, G., Hodgson, C., Warchola, T., Mloszewska, A. M., et al. (2017). Microbe-clay interactions as a mechanism for the preservation of organic matter and trace metal biosignatures in black shales. *Chem. Geol.* 459, 75–90. doi:10.1016/j.chemgeo.2017.04.007

Pollack, J. B., Colburn, D. S., Flasar, F. M., Kahn, R., Carlston, C. E., and Pidek, D. (1979). Properties and effects of dust particles suspended in the Martian atmosphere. *J. Geophys. Res. Solid Earth* 84 (B6), 2929–2945. doi:10.1029/JB084iB06p02929

Poulet, F., Bibring, J. P., Mustard, J. F., Gendrin, A., Mangold, N., Langevin, Y., et al. (2005). Phyllosilicates on Mars and implications for early Martian climate. *Nature* 438 (7068), 623–627. doi:10.1038/nature04274

Quantin-Nataf, C., Carter, J., Mandon, L., Thollot, P., Balme, M., Volat, M., et al. (2021). Oxia Planum: the landing site for the ExoMars "Rosalind Franklin" rover mission: geological context and prelanding interpretation. *Astrobiology* 21 (3), 345–366. doi:10.1089/ast.2019.2191

Raiswell, R. (1987). Non-steady state microbiological diagenesis and the origin of concretions and nodular limestones. *Geol. Soc. Lond. Spec. Publ.* 36 (1), 41–54. doi:10.1144/GSL.SP.1987.036.01.05

Rampe, E. B., Blake, D. F., Bristow, T. F., Ming, D. W., Vaniman, D. T., Morris, R. V., et al. (2020). Mineralogy and geochemistry of sedimentary rocks and eolian sediments in Gale crater, Mars: a review after six Earth years of exploration with Curiosity. *Geochemistry* 80 (2), 125605. doi:10.1016/j.chemer.2020.125605

Rampe, E. B., Ming, D. W., Blake, D. F., Bristow, T. F., Chipera, S. J., Grotzinger, J. P., et al. (2017). Mineralogy of an ancient lacustrine mudstone succession from the Murray formation, Gale crater, Mars. *Earth Planet. Sci. Lett.* 471, 172–185. doi:10.1016/j.epsl.2017.04.021

Rapin, W., Dromart, G., Clark, B. C., Schieber, J., Kite, E. S., Kah, L. C., et al. (2023). Sustained wet–dry cycling on early Mars. *Nature* 620 (7973), 299–302. doi:10.1038/s41586-023-06220-3

Robinson, P., and Luttrell, G. W. (1985). Revision of some stratigraphic names in central Massachusetts. *US Geological Survey Bulletin*, Reston, VA, USA: U.S. Geological Survey, U.S. Dept. of the Interior, 1605-A, A71–A78.

Rull, F., Maurice, S., Hutchinson, I., Moral, A., Perez, C., Diaz, C., et al. (2017). The Raman laser spectrometer for the ExoMars rover mission to Mars. *Astrobiology* 17 (6-7), 627–654. doi:10.1089/ast.2016.1567

Scheller, E. L., Razzell Hollis, J., Cardarelli, E. L., Steele, A., Beegle, L. W., Bhartia, R., et al. (2022). Aqueous alteration processes in Jezero crater, Mars—implications for organic geochemistry. *Science* 378 (6624), 1105–1110. doi:10.1126/science.abo5204

Schlische, R. W. (1993). Anatomy and evolution of the Triassic-Jurassic continental rift system, eastern North America. *Tectonics* 12 (4), 1026–1042. doi:10.1029/93TC01062

Schopf, J. W., Farmer, J. D., Foster, I. S., Kudryavtsev, A. B., Gallardo, V. A., and Espinoza, C. (2012). Gypsum-permineralized microfossils and their relevance to the search for life on Mars. *Astrobiology* 12 (7), 619–633. doi:10.1089/ast.2012.0827

Schreiber, B. C., Philp, R. P., Benali, S., Helman, M. L., De la Peña, J. A., Marfil, R., et al. (2001). Characterisation of organic matter formed in hypersaline carbonate/evaporite environments: hydrocarbon potential and biomarkers obtained through artificial maturation studies. *J. petroleum Geol.* 24 (3), 309–338. doi:10.1111/j.1747-5457.2001.tb00677.x

Schwenzer, S. P., Bridges, J. C., Wiens, R. C., Conrad, P. G., Kelley, S. P., Leveille, R., et al. (2016). Fluids during diagenesis and sulfate vein formation in sediments at Gale crater, Mars. *Meteorit. and Planet. Sci.* 51 (11), 2175–2202. doi:10.1111/maps.12668

Sefton-Nash, E., and Vago, J. L. (2024). “ExoMars/rosalind Franklin mission update,” in *European planetary science congress*, EPSC2024–EPSC2856. doi:10.5194/epsc2024-856

Sefton-Nash, E., Vago, J. L., Joudrier, L., Haessig, F., Williams, A., Mitschdoerfer, P., et al. (2021). “ExoMars 2022 rover science operations preparations,” in European Planetary Science Congress 2021, 13–24 Sep 2021. doi:10.5194/epsc2021-773

Seilacher, A. (2001). Concretion morphologies reflecting diagenetic and epigenetic pathways. *Sediment. Geol.* 143 (1-2), 41–57. doi:10.1016/S0037-0738(01)00092-6

Shkolyar, S., and Farmer, J. D. (2018). Biosignature preservation potential in Playa evaporites: impacts of diagenesis and implications for Mars exploration. *Astrobiology* 18 (11), 1460–1478. doi:10.1089/ast.2018.1849

Siebach, K. L., Grotzinger, J. P., Kah, L. C., Stack, K. M., Malin, M., Léveillé, R., et al. (2014). Subaqueous shrinkage cracks in the Sheepbed mudstone: implications for early fluid diagenesis, Gale crater, Mars. *J. Geophys. Res. Planets* 119 (7), 1597–1613. doi:10.1002/2014JE004623

Simon, J. I., Amundsen, H. E. F., Beegle, L. W., Bell, J., Benison, K. C., Berger, E. L., et al. (2022). “Sampling of Jezero crater máaz formation by mars 2020 perseverance rover,” in *53rd lunar and planetary science conference (LPSC)*.

Squyres, S. W., Arvidson, R. E., Bell III, J. F., Calef III, F., Clark, B. C., Cohen, B. A., et al. (2012). Ancient impact and aqueous processes at endeavour crater, mars. *Science* 336 (6081), 570–576. doi:10.1126/science.1220476

Stack, K. M., Grotzinger, J. P., Kah, L. C., Schmidt, M. E., Mangold, N., Edgett, K. S., et al. (2014). Diagenetic origin of nodules in the sheepbed member, yellowknife bay formation, Gale crater, mars. *J. Geophys. Res. Planets* 119 (7), 1637–1664. doi:10.1002/2014JE004617

Stack, K. M., Grotzinger, J. P., Lamb, M. P., Gupta, S., Rubin, D. M., Kah, L. C., et al. (2019). Evidence for plunging river plume deposits in the Pahrump Hills member of the Murray formation, Gale crater, Mars. *Sedimentology* 66 (5), 1768–1802. doi:10.1111/sed.12558

Stack, K. M., Gupta, S., Tebolt, M., Caravaca, G., Ives, E., Russell, P., et al. (2023). “Sedimentology and stratigraphy of the lower delta sequence, Jezero crater, mars,” in *Lunar and planetary science conference*.

Stack, K. M., Ives, L. R., Gupta, S., Lamb, M. P., Tebolt, M., Caravaca, G., et al. (2024). Sedimentology and stratigraphy of the Shenandoah Formation, western fan, Jezero crater, mars. *J. Geophys. Res. Planets* 129 (2), e2023JE008187. doi:10.1029/2023JE008187

Thomas, N., Markiewicz, W. J., Sablotny, R. M., Wuttke, M. W., Keller, H. U., Johnson, J. R., et al. (1999). The color of the Martian sky and its influence on the illumination of the Martian surface. *J. Geophys. Res. Planets* 104 (E4), 8795–8808. doi:10.1029/98JE02556

Treiman, A. H., Lanza, N. L., VanBommel, S., Berger, J., Wiens, R., Bristow, T., et al. (2023). Manganese-iron phosphate nodules at the Groken site, Gale crater, Mars. *Minerals* 13 (9), 1122. doi:10.3390/min13091122

Udry, A., Ostwald, A., Sautter, V., Cousin, A., Beyssac, O., Forni, O., et al. (2023). A Mars 2020 perseverance SuperCam perspective on the igneous nature of the Máaz formation at Jezero crater and link with Séítah, Mars. *J. Geophys. Res. Planets* 128 (7), e2022JE007440. doi:10.1029/2022JE007440

Vago, J., Witasse, O., Svedhem, H., Baglioni, P., Haldemann, A., Gianfiglio, G., et al. (2015). ESA ExoMars program: the next step in exploring Mars. *Sol. Syst. Res.* 49, 518–528. doi:10.1134/S0038094615070199

Vago, J. L., Westall, F., Coates, A. J., Jaumann, R., Korablev, O., Ciarletti, V., et al. (2017). Habitability on early mars and the search for biosignatures with the ExoMars rover. *Astrobiology* 17 (6-7), 471–510. doi:10.1089/ast.2016.1533

Vaniman, D. T., Martínez, G. M., Rampe, E. B., Bristow, T. F., Blake, D. F., Yen, A. S., et al. (2018). Gypsum, bassanite, and anhydrite at Gale crater, Mars. *Am. Mineralogist J. Earth Planet. Mater.* 103 (7), 1011–1020. doi:10.2138/am-2018-6346

Vasavada, A. R. (2022). Mission overview and scientific contributions from the Mars Science Laboratory Curiosity rover after eight years of surface operations. *Space Sci. Rev.* 218 (3), 14. doi:10.1007/s11214-022-00882-7

Veneranda, M., Saiz, J., Lopez-Reyes, G., Sanz-Arranz, A., Manrique, J. A., Medina, J., et al. (2021). Planetary Terrestrial Analogues Library (PTAL): online database platform and spectroscopic tools. *European Planetary Science Congress 2021*. (15), EPSC2021-105. doi:10.5194/epsc2021-105

Westall, F., Foucher, F., Bost, N., Bertrand, M., Loizeau, D., Vago, J. L., et al. (2015). Biosignatures on Mars: what, where, and how? Implications for the search for martian life. *Astrobiology* 15 (11), 998–1029. doi:10.1089/ast.2015.1374

Williams, R. M., Grotzinger, J. P., Dietrich, W. E., Gupta, S., Sumner, D. Y., Wiens, R. C., et al. (2013). Martian fluvial conglomerates at Gale crater. *science* 340 (6136), 1068–1072. doi:10.1126/science.1237317

Yen, A. S., Ming, D. W., Vaniman, D. T., Gellert, R., Blake, D. F., Morris, R. V., et al. (2017). Multiple stages of aqueous alteration along fractures in mudstone and sandstone strata in Gale Crater, Mars. *Earth Planet. Sci. Lett.* 471, 186–198. doi:10.1016/j.epsl.2017.04.033